J. Fluid Mech. (2009), *vol.* 638, *pp.* 305–337.
doi:10.1017/S0022112009990966

Asymptotic and numerical study of variable-density premixed flame propagation in a narrow channel

MARK SHORT[1]† AND DAVID A. KESSLER[2]

[1]Shock and Detonation Physics Group, Los Alamos National Laboratory, Los Alamos, NM 87545, USA

[2]Laboratory for Computational Physics and Fluid Dynamics, Naval Research Laboratory, 4555 Overlook Avenue, SW Washington, DC 20375, USA

(Received 18 June 2008; revised 26 June 2009; accepted 1 July 2009; first published online 29 September 2009)

The influence of thermal expansion on the dynamics of thick to moderately thick premixed flames (flame thickness less than or comparable to the channel height) for a variable-density flow in a narrow, rectangular channel is explored. The study is conducted within the framework of the zero-Mach-number, variable-density Navier–Stokes equations. Both adiabatic and non-adiabatic channel walls are considered. A small Péclet number asymptotic solution is developed for steady, variable-density flame propagation in the narrow channel. The dynamics of channel flames are also examined numerically for $O(1)$ Péclet numbers in configurations which include flame propagation in a semi-closed channel from the closed to the open end of the channel, flame propagation in a semi-closed channel towards the closed end of the channel and flame propagation in an open channel in which a Poiseuille flow (flame assisting or flame opposing) is imposed at the channel inlet. Comparisons of the finite-Péclet-number dynamics are made with the behaviour of the small-Péclet-number solutions. We also compare how thermal expansion modifies the flow dynamics from those determined by a constant-density model. The small-Péclet-number variable-density solution for a flame propagating in a circular pipe is given in the Appendix.

1. Introduction

The propagation of premixed flames in narrow channels or tubes is an important topic in several areas of combustion research. Emerging technologies such as the development of microscale combustors as a power source for portable devices (e.g. laptops or cell phones) depend on this type of configuration (Jones, Lloyd & Weinberg 1978; Fernandez-Pello 2002). Likewise, flame propagation in confined narrow channels is relevant to the issue of control of flashback in burners with an injectable mass flux. For micro-combustion technologies, the extension of flammability limits for flames in narrow channels by minimizing heat losses is essential. For channels of decreasing height, quenching arises due to the increase in surface area to volume ratio (Lewis & von Elbe 1961; Jones, Lloyd & Weinberg 1978; Williams 1985). For channel flame propagation parallel to the wall, two modes of flame extinction are known to exist. In sufficiently wide channels, partial extinction of the flame in the near-wall

† Email address for correspondence: short1@lanl.gov

region occurs, typically over a region around six times the laminar flame thickness (Clendening, Shackleford & Hilyard 1981; Daou & Matalon 2002). In narrower channels total flame quenching can occur (Lewis & von Elbe 1961). With relevance to micro-burner applications, the purpose of the present paper is to examine how the flow field induced by thermal expansion affects the flame shape, burning rate and quenching limits in either a semi-closed channel or open channel with a Poiseuille flow imposed at the inlet, in the limit in which the flame thickness is smaller than, or of the same order, as the channel height.

Of most relevance to the current study are the studies of Daou & Matalon (2001, 2002). They studied the mass burning-rate variation of symmetric flames in narrow rectangular channels in a thermo-diffusive model subject to an imposed flow field of Poiseuille form. Adiabatic channel walls were considered in Daou & Matalon (2001) and non-adiabatic walls in Daou & Matalon (2002). Asymptotic representations of the burning rate were obtained in the limit of weak flows and where the laminar flame thickness was either much longer (thick flames) or shorter (thin flames) than the height of the channel. For adiabatic walls, a flame either assisted or opposed by a Poiseuille flow resulted in an increase in the flame curvature due to stretch and hence an increase in the burning rate. The burning rate increased with the magnitude of the Poiseuille flow. Thin flames were found to develop more surface area when opposed by the flow, and consequently a higher burning rate, than a flow-assisted flame with the same flow intensity. In the limit of very thick flames, the axial flame speed was found to be smaller (for flow-opposed flames) or larger (for flow-assisted flames) than the laminar flame speed by the average cross-sectional speed of the Poiseuille flow. Also, in the thick-flame limit, the leading-order magnitude of the spatial flame deformation induced by the flow was found to be identical for a flame-opposed or flame-assisted flow of the same magnitude.

For non-adiabatic walls, Daou & Matalon (2002) conducted an asymptotic analysis of the structure of thick flames subject to a fixed Poiseuille flow. Provided the convective heat transfer (loss) parameter was of the order of the square of the ratio of the channel height to the laminar flame thickness, the flame structure was found to be one-dimensional with a mass burning rate associated with a one-dimensional flame having a volumetric heat loss equivalent to that at the channel walls. Consequently, a critical value of the scaled heat transfer parameter could be identified that resulted in quenching. For moderate Péclet numbers, flow-opposed non-adiabatic flames were found to be more sensitive to heat loss than flow-assisted flames. Flames in sufficiently wide channels were not globally quenched, but undergo local quenching in the wall vicinity for sufficiently large heat losses. Later work examined the effect of non-unity Lewis numbers (Kurdyumov & Fernandez-Tarrazo 2002; Cui, Matalon & Jackson 2005) for thin and thick flames. In particular, for thick flames, non-unity Lewis numbers were found to play a minor role.

Using a large activation energy, near equi-diffusional formulation, Cui *et al.* (2004) were able to extend the analysis of the non-adiabatic thick-flame structure (Daou & Matalon 2002) to an additional order in the ratio of the channel height to flame thickness. At this order, for adiabatic walls, it was found that the burning rate is enhanced uniformly regardless of the direction of the imposed flow. However, in the presence of heat losses, the thick-flame burning rate depended on the direction of the flow, with generally a higher burning rate identified for flow-assisted flames than flow-opposed flames. The effects of heat loss on the spatial deformation of the thick flame are also quantified at this additional order. With no imposed flow, the flame is found to be convex towards the unburned gases.

The constant density model (CDM) used in Daou & Matalon (2001) and Daou & Matalon (2002) does not provide for flow field modifications induced by thermal expansion due to combustion. In practice, thermal expansion of the hot combustion gases in narrow channels will induce a flow, which could have significant implications for channel flame propagation. For example, accelerating flames that propagate from the closed to the open end of a narrow tube have been been identified and characterized by Ott, Oran & Anderson (2003) and Gamezo & Oran (2006) via numerical solution of the compressible Navier–Stokes equations. The acceleration was attributed to interaction, and resulting stretching, of the flame with a velocity gradient in a thin boundary layer along the channel wall. The formation of the boundary layer was a direct result of an upstream flow generated by thermal-expansion-induced flow. Dobrego, Kozlov & Vasiliev (2006) have also examined the dependence of flame acceleration on the width of a semi-closed tube after ignition at the closed end of the tube. There have also been several numerical studies conducted on the nature of flame propagation in channels or pipes in the context of either the variable density or compressible reactive Navier–Stokes equations. Hackert, Ellzey & Ezekoye (1998) have examined the dependence of flame shape and quenching in ducts with either isothermal, adiabatic or convectively and radiatively cooled walls. In addition to the role of thermal boundary conditions in determining the shape and speed of flames propagating in narrow channels, Kim & Maruta (2006) also numerically examined the role of the shape and magnitude of the channel inlet flow. Tsai (2008) has also examined the preference for a duct confined flame to propagate as an asymmetric or symmetric structure.

For narrow channels, the role of axial heat conduction along the heated confining walls of the channel can also have a significant influence on the combustion stability limits, particularly so when the flame is stationary or slowly propagating relative to the channel walls. The wall heating can be due to an external source, or from internal heating due to combustion in the channel. The effects of axial wall heat conduction on the propagation and stability limits of combustion in narrow channels have been examined in a number of recent papers (e.g. Zamashchikov 2001; Zamashchikov & Minaev 2001; Norton & Vlachos 2003; Ronney 2003; Miesse *et al.* 2004; Ju & Xu 2005; Leach & Cadou 2005; Maruta *et al.* 2005; Chao *et al.* 2007; Jackson *et al.* 2007; Mineav, Maruta & Fursenko 2007; Kessler & Short 2008). The influence of axial wall heat conduction on the configuration studied in the present paper is considered in a separate paper (Short & Kessler submitted).

The present paper extends the work on the dynamics of thick and moderately thick flames (flame thickness less than or comparable to the channel height) of Daou & Matalon (2001, 2002) to variable-density flows. Thus, amongst other issues, we describe how the flow induced by thermal expansion affects the shape and propagation of thick and moderately thick flames in both a semi-closed channel and an open channel with an imposed inlet Poiseuille flow and how total flame extinction by excessive heat losses in a narrow channel is affected by the flow modification. A small Péclet number variable-density asymptotic solution is also developed, which provides valuable insights into how thermal expansion affects the shape, propagation and quenching of thick and moderately thick flames. In § 2, the model framework is established. The small-Péclet-number asymptotic solution is developed in § 3. In § 4, the dynamics of narrow-channel flames are examined for $O(1)$ Péclet numbers for both adiabatic and non-adiabatic configurations, and comparisons made with the small-Péclet-number flame dynamics. A study on how thermal expansion modifies the flow dynamics from those of a CDM (Daou & Matalon 2001, 2002) is also

conducted. In Appendix A, the small-Péclet-number variable-density solution for a flame propagating in a circular pipe is given.

2. Model

Premixed flame propagation in a two-dimensional channel bounded by inert walls is considered (figure 1). The effects of thermal expansion are considered through the variable-density Navier–Stokes equations in the zero-Mach-number limit. In non-dimensional form, and for a one-step reaction mechanism, these are

$$\frac{\mathrm{D}\rho}{\mathrm{D}t} = -\rho(\nabla\cdot\boldsymbol{u}), \quad \rho\frac{\mathrm{D}u_i}{Dt} = -\nabla p + \frac{1}{Re}\nabla\cdot\tau, \quad \rho T = 1, \tag{2.1a–c}$$

$$\rho\frac{\mathrm{D}T}{\mathrm{D}t} = \frac{1}{Pe}\nabla^2 T + QPeR, \quad \rho\frac{\mathrm{D}Y}{\mathrm{D}t} = \frac{1}{LePe}\nabla^2 Y - PeR, \tag{2.1d,e}$$

where

$$\tau_{ij} = \frac{\partial u_j}{\partial x_i} + \frac{\partial u_i}{\partial x_j} - \frac{2}{3}\delta_{ij}\left(\frac{\partial u_k}{\partial x_k}\right), \tag{2.2}$$

for temperature T $(=\tilde{T}/\tilde{T}_r)$, fluid velocity $u_i=(u,v)$ $(=\tilde{u}_i/\tilde{s}_F)$, density ρ $(=\tilde{\rho}/\tilde{\rho}_r)$, pressure $p=([\tilde{p}-\tilde{p}_r]/\tilde{\rho}_r\tilde{s}_F^2)$ and fuel mass fraction Y $(=\tilde{Y}/\tilde{Y}_r)$. The temperature scale $\tilde{T}_r$ $(=300K)$ is set so that $T=1$ in the fresh mixture (where $Y=1$), while $\tilde{s}_F$ is the laminar flame speed and $\tilde{\rho}_r=\tilde{p}_r/(\tilde{R}\tilde{T}_r/\tilde{W})$, where $\tilde{p}_r$ is the pressure at the channel outlet. The length scale is the half-channel height $\tilde{a}$, and the time scale is $\tilde{a}/\tilde{s}_F$. The non-dimensional groups are the Péclet number Pe $(=PrRe$, where the Reynolds number $Re=\tilde{\rho}_r\tilde{s}_F\tilde{a}/\tilde{\mu}$ and the Prandtl number $Pr=\tilde{\mu}\tilde{c}_p/\tilde{\lambda})$, the Lewis number $Le=\tilde{\lambda}/\tilde{c}_p\tilde{\rho}\tilde{\mathscr{D}}$ and the heat release $Q=\tilde{Q}\tilde{Y}_r/\tilde{c}_p\tilde{T}_r$. Here $\tilde{\mu}$, $\tilde{c}_p$, $\tilde{Q}$, $\tilde{R}$ and $\tilde{\lambda}$ are the dimensional dynamic viscosity, specific heat, heat of formation, the gas constant and the thermal conductivity. In the present study, they are taken to be constant. The reaction rate is

$$R = D\rho Y\exp(-\theta/T), \tag{2.3}$$

where the Damköhler number $D=\tilde{D}\tilde{D}_{TH}/\tilde{s}_F^2$ and the activation energy $\theta=\tilde{E}/\tilde{R}\tilde{T}_r$. The thermal diffusivity $\tilde{D}_{TH}=\tilde{\lambda}/\tilde{\rho}_r\tilde{c}_p$, while $\tilde{D}$ and $\tilde{E}$ are the dimensional pre-exponential factor and activation energy.

Symmetry conditions

$$\frac{\partial T}{\partial y}=0, \quad \frac{\partial Y}{\partial y}=0, \quad \frac{\partial u}{\partial y}=0, \quad v=0, \quad \frac{\partial p}{\partial y}=0, \tag{2.4a–e}$$

are applied along the centreline $(y=1)$, thus restricting our solutions to symmetric ones. Cases in which the channel wall $(y=0)$ is either adiabatic or non-adiabatic are examined. In general, along $y=0$,

$$\frac{\partial T}{\partial y}=k(T-1), \quad \frac{\partial Y}{\partial y}=0, \quad u=0, \quad v=0, \tag{2.5a–d}$$

where k is a heat loss coefficient. Two different channel inlet/exit configurations are considered. In one case (figure 1), a fully developed Poiseuille inflow at the inlet $x=0$ is imposed, where

$$T=1, \quad Y=1, \quad u=u_c(2y-y^2), \quad v=0, \tag{2.6a–d}$$

with $\mathrm{d}p/\mathrm{d}x=-2u_c/Re$. Here u_c is the axial velocity amplitude on the centreline $(y=1)$ at $x=0$. The channel exit (at $x=L$) is open to the atmosphere, with a channel

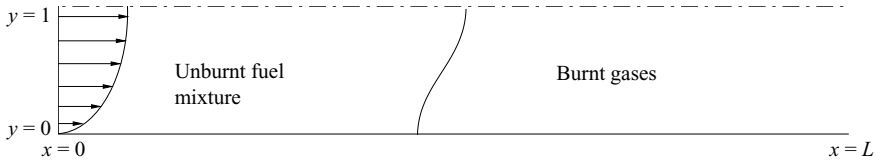

FIGURE 1. Schematic of the channel configuration for the variable-density Navier–Stokes simulations. The line $y=0$ is the channel wall, while $y=1$ is a flow symmetry boundary.

length that is sufficiently long for the flow to relax to a unidirectional one at $x=L$. Then

$$\frac{\partial T}{\partial x}=0, \quad \frac{\partial Y}{\partial x}=0, \quad \frac{\partial u}{\partial x}=0, \quad \frac{\partial v}{\partial x}=0, \quad p=0, \tag{2.7a–d}$$

at $x=L$. In the other case, either flame propagation away from a closed channel wall (at $x=L$) towards an open channel (at $x=0$) or flame propagation towards a closed channel wall (at $x=0$) is considered. In each case, a flow is not imposed at the open boundary. The conditions

$$\frac{\partial T}{\partial x}=\pm k(T-1), \quad \frac{\partial Y}{\partial x}=0, \quad u=0, \quad v=0 \tag{2.8a–d}$$

are imposed at the closed end of the channel, with the plus or minus sign in (2.8a) respectively assigned according to whether the closed wall is at $x=0$ or $x=L$. Conditions (2.7) are applied at the open boundary.

One of the main diagnostics used in this paper is the burning rate Ω in the channel (across $y=0$ to $y=1$), defined as

$$\Omega = Pe \int_{x=0}^{L}\int_{y=0}^{1} R \,\mathrm{d}x\,\mathrm{d}y. \tag{2.9}$$

This quantity is equivalent to the dimensional average mass consumed in the channel per unit time and unit breadth and height relative to that consumed by a one-dimensional flame moving at the laminar speed. Finally, the constant-density flame channel propagation model (Daou & Matalon 2002) used below for comparison with the variable-density behaviour is obtained from (2.1d,e) by setting $\rho=1$, $u=u_c(2y-y^2)$ and $v=0$.

3. $Pe\to 0$ analysis for rectangular channel flow

The solution for a variable-density flame propagating steadily in a rectangular channel is now derived in the limit in which the channel height is smaller than the flame thickness, i.e. in which $Pe\to 0$. The corresponding $Pe\to 0$ solution for flame propagation in a circular pipe is given in Appendix A. We assume that the flame propagates to the left (x decreasing) with constant axial velocity U. In a frame of reference travelling with the axial flame velocity, the axial coordinate is stretched according to

$$\xi = Pe(x+Ut), \tag{3.1}$$

while the pressure is rescaled such that

$$\bar{p} = Pe^2 p, \tag{3.2}$$

where ξ and $\bar{p}$ are $O(1)$. The upstream state is given at $\xi \to -\infty$, while the far downstream state occurs at $\xi = +\infty$. With scales (3.1) and (3.2), (2.1) becomes,

$$Pe\frac{\partial}{\partial\xi}(\rho(u+U)) + \rho\frac{\partial v}{\partial y} + v\frac{\partial\rho}{\partial y} = 0, \tag{3.3a}$$

$$Pe\rho(u+U)\frac{\partial u}{\partial\xi} + \rho v\frac{\partial u}{\partial y} = -\frac{1}{Pe}\frac{\partial\bar{p}}{\partial\xi} + \frac{Pr}{Pe}\left[\frac{4Pe^2}{3}\left(\frac{\partial^2 u}{\partial\xi^2}\right) + \left(\frac{\partial^2 u}{\partial y^2}\right) + \frac{Pe}{3}\left(\frac{\partial^2 v}{\partial\xi\,\partial y}\right)\right], \tag{3.3b}$$

$$Pe\rho(u+U)\frac{\partial v}{\partial\xi} + \rho v\frac{\partial v}{\partial y} = -\frac{1}{Pe^2}\frac{\partial\bar{p}}{\partial y} + \frac{Pr}{Pe}\left[\frac{4}{3}\left(\frac{\partial^2 v}{\partial y^2}\right) + Pe^2\left(\frac{\partial^2 v}{\partial\xi^2}\right) + \frac{Pe}{3}\left(\frac{\partial^2 u}{\partial\xi\,\partial y}\right)\right], \tag{3.3c}$$

$$Pe^2\rho(u+U)\frac{\partial T}{\partial\xi} + Pe\rho v\frac{\partial T}{\partial y} = Pe^2\frac{\partial^2 T}{\partial\xi^2} + \frac{\partial^2 T}{\partial y^2} + Pe^2 QR, \tag{3.3d}$$

$$Pe^2\rho(u+U)\frac{\partial Y}{\partial\xi} + Pe\rho v\frac{\partial Y}{\partial y} = \frac{1}{Le}\left(Pe^2\frac{\partial^2 Y}{\partial\xi^2} + \frac{\partial^2 T}{\partial y^2}\right) - Pe^2 R. \tag{3.3e}$$

The $Pe \to 0$ leading-order behaviour can be obtained by setting

$$T \sim T_0, \quad Y \sim Y_0, \quad u \sim u_0, \quad \bar{p} \sim \bar{p}_0, \quad \rho \sim \rho_0, \quad v \sim Pe\, v_0, \tag{3.4}$$

so that the transverse velocity has an amplitude $O(Pe)$. Consequently,

$$\frac{\partial^2 T_0}{\partial y^2} = 0, \quad \frac{\partial^2 Y_0}{\partial y^2} = 0, \quad \frac{\partial\bar{p}_0}{\partial y} = 0, \quad \frac{\partial\bar{p}_0}{\partial\xi} = Pr\frac{\partial^2 u_0}{\partial y^2}, \quad \rho_0 = \frac{1}{T_0}, \tag{3.5a–e}$$

where, from (3.5c), $\bar{p}_0 = \bar{p}_0(\xi)$. Integrating the temperature equation (3.5a), and applying the symmetry condition (2.4a), gives $\partial T_0/\partial y = 0$. For compatibility, the heat loss coefficient k in the thermal wall condition (2.5a) must have therefore an amplitude $k = o(1)$. The specific order of k can be calculated as in Daou & Matalon (2002). Recognizing that $\partial T/\partial y \ll 1$, (3.3$e$) can be integrated across the channel using the mass conservation relation (3.3a) to show that

$$\Omega = \int_{-\infty}^{\infty}\int_0^1 R\,\mathrm{d}y\,\mathrm{d}\xi \sim \frac{k}{QPe^2}\int_{-\infty}^{\infty}(T(\xi,0)-1)\,\mathrm{d}\xi, \tag{3.6}$$

assuming $T \to 1$ and $\partial T/\partial\xi \to 0$ as $\xi \to \pm\infty$ for $k \neq 0$. Thus for $\Omega = O(1)$, $k = O(Pe^2)$. Consequently (2.5a) will be rewritten as

$$\frac{\partial T}{\partial y} = Pe^2\kappa(T-1) \tag{3.7}$$

with $\kappa = O(1)$. Similarly, integrating (3.5b) with inert-wall conditions (2.4b) and (2.5b) gives $\partial Y_0/\partial y = 0$, and thus

$$T \sim T_0(\xi), \quad Y \sim Y_0(\xi); \tag{3.8}$$

i.e. the leading-order temperature and reactant mass fractions have no transverse spatial variation. Additionally, $\rho_0 = \rho_0(\xi)$ as a result of (3.5e). A separable solution for the leading-order axial velocity variation $u_0 = u_0(\xi, y)$ can be constructed in the form

$$u_0 = \hat{u}_0(y)\tilde{u}_0(\xi), \tag{3.9}$$

where, from (2.4*c*) and (2.5*c*), the boundary conditions on $\hat{u}_0(y)$ are

$$\frac{\partial \hat{u}_0}{\partial y}(1) = 0, \quad \hat{u}_0(0) = 0. \tag{3.10}$$

The form of $\hat{u}_0$ is determined from the momentum equation (3.5*d*), where

$$\frac{\partial^2 \hat{u}_0}{\partial y^2} = \frac{1}{Pr\tilde{u}_0}\frac{\partial \bar{p}_0}{\partial \xi} = -2C. \tag{3.11}$$

Thus the axial pressure gradient $\mathrm{d}\bar{p}_0/\mathrm{d}\xi$ can be determined once $\tilde{u}_0(\xi)$ is known. The solution for $\hat{u}_0$ is

$$\hat{u}_0(y) = C(2y - y^2) \tag{3.12}$$

so that

$$u_0(\xi, y) = \tilde{u}_0(\xi)(2y - y^2), \tag{3.13}$$

where the constant C has been absorbed into $\tilde{u}_0$. Consequently, the axial velocity variation in the transverse direction corresponds to channel Poiseuille flow but with a magnitude for each y ($0 < y \leqslant 1$) that varies as a function of the axial coordinate ξ. The mass conservation equation for the leading-order solution can be obtained from (3.3*a*) as

$$\frac{\partial}{\partial \xi}(\rho_0(u_0 + U_0)) + \rho_0\frac{\partial v_0}{\partial y} = 0, \tag{3.14}$$

where $v_0 = v_0(\xi, y)$ and $U \sim U_0$. An integration between $y = 0$ and $y = 1$, in combination with the boundary conditions $v_0(\xi, 0) = v_0(\xi, 1) = 0$ obtained from (2.4*d*) and (2.5*d*), gives

$$\frac{\partial}{\partial \xi}\left(\rho_0\left(\frac{2}{3}\tilde{u}_0 + U_0\right)\right) = 0 \tag{3.15}$$

or

$$\rho_0(\xi)\left(\frac{2}{3}\tilde{u}_0(\xi) + U_0\right) = \left(\frac{2}{3}\tilde{u}_{0u} + U_0\right) = M, \tag{3.16}$$

where

$$\tilde{u}_{0u} = \tilde{u}_0(\xi = -\infty) \tag{3.17}$$

is the centreline ($y = 1$) magnitude of the Poiseuille flow upstream of the flame. Thus M is a mass flux based on a flame propagation speed relative to an observer moving with the average cross-sectional velocity associated with the Poiseuille flow. The $O(Pe)$ transverse velocity becomes

$$v_0 = -\frac{y}{\rho_0}\frac{\partial}{\partial \xi}\left(\rho_0\left(\tilde{u}_0\left(y - \frac{y^2}{3}\right) + U_0\right)\right), \tag{3.18}$$

and the magnitude of the vorticity

$$|\omega| = -\frac{\partial u_0}{\partial y} + O(Pe^2) = -2\tilde{u}_0(1 - y) + O(Pe^2). \tag{3.19}$$

The vorticity is zero on the symmetry axis $y = 1$ and varies linearly with y, its magnitude being proportional to $\tilde{u}_0$.

In order to determine $T_0(\xi)$ and $Y_0(\xi)$, (3.3*d*) and (3.3*e*) at $O(Pe^2)$ are considered, where

$$T \sim T_0(\xi) + Pe^2T_1(\xi, y), \quad Y \sim Y_0(\xi) + Pe^2Y_1(\xi, y). \tag{3.20}$$

Integrating the $O(Pe^2)$ temperature equation

$$\rho_0(\tilde{u}_0(2y-y^2)+U_0)\frac{\partial T_0}{\partial \xi}=\frac{\partial^2 T_0}{\partial \xi^2}+\frac{\partial^2 T_1}{\partial y^2}+QR_0(\xi) \tag{3.21}$$

obtained from (3.3*d*) between $y=0$ and $y=1$ gives

$$\rho_0\left(\frac{2}{3}\tilde{u}_0+U_0\right)\frac{\partial T_0}{\partial \xi}=\frac{\partial^2 T_0}{\partial \xi^2}-\kappa(T_0-1)+QR_0(\xi) \tag{3.22}$$

or

$$M\frac{\partial T_0}{\partial \xi}=\frac{\partial^2 T_0}{\partial \xi^2}-\kappa(T_0-1)+QR_0(\xi). \tag{3.23}$$

Similarly, the $O(Pe^2)$ mass fraction equation

$$\rho_0(u_0+U_0)\frac{\partial Y_0}{\partial \xi}=\frac{1}{Le}\left(\frac{\partial^2 Y_0}{\partial \xi^2}+\frac{\partial^2 Y_1}{\partial y^2}\right)-R_0, \tag{3.24}$$

obtained from (3.3*e*), can be integrated between $y=0$ and $y=1$ to give

$$M\frac{\partial Y_0}{\partial \xi}=\frac{1}{Le}\frac{\partial^2 Y_0}{\partial \xi^2}-R_0. \tag{3.25}$$

It should be noted that equations (3.23) and (3.25) for $T_0(\xi)$ and $Y_0(\xi)$ are essentially identical to those derived by Daou & Matalon (2002) in the $Pe\to 0$ limit for the constant-density approximation. The only difference arises with the choice of R_0 in the variable-density model (VDM). They are the standard equations that determine the spatial structure and propagation velocity of a one-dimensional flame with a volumetric heat loss term (Daou & Matalon 2002). In particular, an increase in κ will result in the attainment of complete quenching. For the adiabatic case ($\kappa=0$), $M=1$ with the scalings used in § 2. In the limit of large activation energy θ, the flux M is

$$M^2\ln\frac{1}{M}=\frac{(T_b-1)\kappa}{\theta T_b^2} \tag{3.26}$$

and the critical heat loss κ_c below which flames are quenched is

$$\kappa_c=\frac{T_b^2}{2e\theta(T_b-1)}. \tag{3.27}$$

The significant difference between the variable- and constant-density cases as $Pe\to 0$ is that the leading-order axial velocity is now modified by the propagating flame in variable-density flow. The implications of this are discussed below for the inlet and exit flow conditions (2.6)–(2.8) specified in § 2.

3.1. *Poiseuille flow at the inlet*

First consider a propagating flame opposed or assisted by a fully developed Poiseuille inlet flow ($\xi\to-\infty$), where

$$u=u_c(2y-y^2) \tag{3.28}$$

(see (2.6*c*)). Then, $\tilde{u}_{0u}=u_c$ and

$$U_0=M-\frac{2}{3}u_c \tag{3.29}$$

so that the axial flame propagation speed is identical in both the variable- and constant-density cases. Blow-off ($U_0<0$) occurs whenever $u_c>3M/2$. However, in the

variable-density case, the axial velocity profile through the channel is $u = \tilde{u}_0(2y - y^2)$, where

$$\tilde{u}_0(\xi) = u_c + \frac{3}{2}M(T_0(\xi) - 1). \tag{3.30}$$

Consequently, $\tilde{u}_0$ far downstream ($\xi \to +\infty$) of the flame is given by

$$\tilde{u}_{0b} = \tilde{u}_0(\xi \to +\infty) = u_c + \frac{3}{2}M(T_{0b} - 1), \tag{3.31}$$

where $T_{0b} = 1 + Q$ in the adiabatic case and $T_{0b} = 1$ in the non-adiabatic case. Thus $\tilde{u}_{0b} = u_c + 3Q/2$ in the adiabatic case, and $\tilde{u}_{0b} = u_c$ in the non-adiabatic case. For flame propagation towards the closed end of a channel, where $u = 0$ as $\xi \to -\infty$, a similar discussion is appropriate but where $u_c = 0$.

3.2. *Semi-closed channel, propagation away from the closed end*

For flame propagation away from the closed end of a tube, $\tilde{u}_{0b} = 0$ as $\xi \to +\infty$. For an adiabatic channel, thermal expansion will then induce a flow upstream of the flame, where $u = u_i(2y - y^2)$ as $\xi \to \infty$. Based on (3.31), the magnitude of the centreline ($y = 1$) axial velocity must then be

$$u_i = -\frac{3Q}{2}. \tag{3.32}$$

Consequently, the axial flame propagation speed is

$$U_0 = 1 + Q. \tag{3.33}$$

In the adiabatic CDM, in order that the downstream axial flow velocity be zero ($\tilde{u}_b = 0$), we must set $u_c = 0$ in (2.1*d*,*e*). In this case, $U_0 = 1$. On the other hand, in order for the flame speed in the CDM to match that of the variable-density prediction for a flame propagating away from a closed wall in an adiabatic channel when $Pe \to 0$, the flame in the CDM should be assisted by an imposed Poiseuille flow of the form $u = -3Q(2y - y^2)/2$. The consequences of making these two choices in the CDM in comparison with the VDM behaviour are ascertained in § 4. For a flame propagating away from a closed wall in the non-adiabatic variable-density case, there is no induced flow far upstream of the flame, and thus $U = M$, which coincides with the non-adiabatic result that one obtains from the CDM having no imposed flow.

3.3. *Axial flow variation*

Equations (3.30) and (3.31) also tell us about the direction and magnitude of the axial flow variation through the flame. Consider the adiabatic case first. When $u_c \geqslant 0$, $\tilde{u}_0(\xi)$ increases monotonically through the flame reaching the value $u_c + 3Q/2$. For $u_c < 0$, $\tilde{u}$ increases towards zero and reverses sign at $T_0(\xi) = 1 - 2u_c/3$ provided that $1 - 2u_c/3 < 1 + Q$ or $u_c > -3Q/2$. The quantity $\tilde{u}_0$ again reaches the value $u_c + 3Q/2$ when the reactant is depleted. The magnitude of $\tilde{u}_0$ in the burnt-gas flow equals $-u_c$ when $u_c = -3Q/4$. For $u_c < -3Q/2$, the burnt-gas flow is in the direction of the imposed outflow. More complex behaviours can occur for the non-adiabatic case. For $u_c > 0$, $\tilde{u}_0$ increases for $\xi < \xi_m$, where ξ_m is the value of ξ at which T_0 obtains its maximum and subsequently decreases to the value u_c for $\xi > \xi_m$. For $u_c < 0$, $\tilde{u}_0$ increases towards zero, changing signs when $T_0 = 1 - 2u_c/(3M)$, provided $\max[T_0] > 1 - 2u_c/(3M)$. The quantity $\tilde{u}_0$ reaches a maximum value $u_c + 3M(\max[T_0] - 1)/2$, upon which it decreases in magnitude, reverses direction and subsequently relaxes to u_c. When $\max[T_0] \leqslant 1 - 2u_c/(3M)$, $\tilde{u}_0$ will first increase and subsequently decrease to u_c with no change in the flow direction.

3.4. $O(Pe^2)$ mass fraction surface perturbation

Finally, as in Daou & Matalon (2002), it is insightful to calculate the $O(Pe^2)$ modification to the flame shape, in this case to each surface of fixed Y, that occurs due to the non-planar flow. The $O(Pe^2)$ variation in Y can be obtained by integrating the $O(Pe^2)$ reactant mass equation (3.3*e*) in y using $\partial Y/\partial y = 0$ (2.4*b*) on $y = 1$. A further integration in y together with the leading-order result $Y_0(\xi)$ yields

$$Y \sim Y_0(\xi) + Pe^2 Le \left(-\frac{\rho_0 \tilde{u}_0}{12} y^2 (y-2)^2 \frac{\partial Y_0}{\partial \xi} + A(\xi) \right). \tag{3.34}$$

Now let ξ^* be the location at which Y has the value Y^* in the leading-order description. The $O(Pe^2)$ perturbation to the position at which Y now attains the constant-mass fraction Y^* is given by

$$\xi = \xi^* + Pe^2 \xi', \tag{3.35}$$

where

$$\xi' = \frac{Le \rho_0 \tilde{u}_0}{12} y^2 (y-2)^2 + B(\xi^*). \tag{3.36}$$

Consequently, the relative distance between the reactant mass fraction reaching the value Y^* on $y = 0$ and reaching the value Y^* on $y = 1$, a measure of the flame deformation due to the flow, is given by

$$\xi_r' = \frac{Le \rho_0 \tilde{u}_0}{12}. \tag{3.37}$$

Each surface of constant-mass fraction is thus concave towards the upstream when $\tilde{u}_0 > 0$ and convex for $\tilde{u}_0 < 0$. Note that the corresponding result for the CDM (Daou & Matalon 2002) has $\xi_r' = Le\, u_c/12$. Also, from (3.16), the mass flux $\rho_0 \tilde{u}_0$ is given by

$$\rho_0 \tilde{u}_0 = u_c + \frac{3U_0}{2}(1 - \rho_0), \tag{3.38}$$

or, equivalently,

$$\rho_0 \tilde{u}_0 = \rho_0 u_c + \frac{3}{2} M (1 - \rho_0), \tag{3.39}$$

where M is constant.

Several implications of the results (3.38) and (3.39) are worth noting. First, as in Daou & Matalon (2002), neither the effects of heat loss nor those of Lewis number variations close to one determine the $O(Pe^2)$ spatial perturbation to the surfaces of constant-mass fraction. A study of their effects in the constant-density formulation, which enter at $O(Pe^4)$, was conducted by Cui *et al.* (2004). Also, since $\rho_0 < 1$, when $u_c > 0$, $\rho_0 \tilde{u}_0 > u_c$ for $U_0 > 0$ (i.e. for $u_c < 3M/2$) from (3.38). As a result, the deformation experienced by each surface of constant-mass fraction under variable-density conditions will be larger than that found under the CDM, and thus one would expect higher burning rates with the variable-density flow. On the other hand, under blow-off conditions, i.e. for $U_0 < 0$ ($u_c > 3M/2$), $\rho_0 \tilde{u}_0 < u_c$ and both the flame deformation and the burning rate experienced under a variable-density flow should be smaller than that found for the corresponding constant-density approximation. When $u_c < 0$ the effects of the relative deformation experienced by each surface of constant-mass fraction is more difficult to quantify, since $\tilde{u}_0$ can change sign through the flame. For $T_0 < 1 - 4u_c/(3M)$, (i.e. when $|u_c| > |u_0|$), each surface of constant-mass fraction in the variable-density flow will experience less relative deformation than its constant-density counterpart. For $T_0 > 1 - 4u_c/(3M)$ the opposite is true. Thus, for

instance, in an adiabatic channel when $u_c < -3Q/2$ (where no reversal in the direction of the flow occurs through the flame), the constant-density flame must have a higher burning rate. In contrast, for sufficiently small u_c (< 0), the variable-density flame will experience significantly more deformation than the corresponding constant-density flame due to fluid expansion, and thus the variable-density flame should have a higher burning rate.

The flame deformation result, $\xi_r' = Le\, u_c/12$, obtained by Daou & Matalon (2002) also implies that for the constant-density approximation, the relative magnitude of deformation experienced by each surface of constant-mass fraction is identical for a flow of the same magnitude being directed either into the channel ($u_c > 0$) or out of the channel ($u_c < 0$). For variable-density flow, this is not the case. Result (3.39) shows that since $3M(1-\rho_0)/2 > 0$, the relative deformation experienced by a flame opposed by a flow of magnitude u_c (> 0) is greater than that for a flame assisted by a flow of the same magnitude u_c ($u_c < 0$), so that the burning rate for flow-assisted flames should be smaller than for flow-opposed flames. Also, based on the above discussion of the variation in $\tilde{u}_0$ (3.30), the flame structure in a variable-density flow may consist of a combination of surfaces of constant-mass fraction that are either convex or concave to the upstream flow. For instance, in an adiabatic assisted flow with $0 > u_c > -3Q/2$, the reaction surfaces with $\tilde{u}_0 < 0$ will be convex to the upstream while those with $\tilde{u}_0 > 0$ will be concave. In a non-adiabatic assisted flow, if $\max[T_0] > 1 - 2u_c/(3M)$, the head of the flame will be convex, with a change to concave surfaces of constant-mass fraction when $T_0 = 1 - 2u_c/(3M)$. A further switch to convex surfaces at the rear of the flame may occur depending on the heat loss. Finally, we note that an increase in u_c (with $u_c > 0$) leads to higher deformation magnitudes $\rho_0\tilde{u}_0$ for each surface of constant-mass fraction and thus to higher burning rates. The situation for $u_c < 0$ is again more complex. In the adiabatic case, decreases in u_c below $u_c = -3Q/2$ will lead to higher burning rates. When $0 > u_c > -3Q/2$, where flow reversal occurs through the flame, the effect of changing u_c on the burning rate is difficult to ascertain. This is investigated numerically below.

4. Results: the effects of thermal expansion on premixed flame propagation in narrow channels

4.1. *Numerical procedure for the calculation of the variable-density solutions*

For the variable-density calculations shown below, (2.1)–(2.8) are solved using a method based on a fractional-step pressure-correction finite-difference scheme on a staggered grid. Spatial derivatives are calculated using second-order central-difference schemes, and a predictor–corrector time advancement scheme is employed to achieve second-order accuracy in time. The details of the implementation have been described by Liu (2003) and Kessler (2006). A typical grid spacing in the axial direction was 0.0275, while that in the transverse was 0.02. These were sufficient to convergently resolve the small-Péclet-number to moderate-Péclet-number flame structures and flow fields examined below. To ignite the mixture at $t = 0$, a pocket of hot burnt gas with radius $r_0 = 1$ is placed in the channel such that $T = 1$ and $Y = 1$ for $r^2 > r_0^2$ and $T = 1 + \beta Q \exp(-r^2)$ and $Y = 1 - \exp(-r^2)$ for $r^2 < r_0^2$, where $r^2 = (x-x_0)^2 + (y-1)^2$. For adiabatic channels $\beta = 1$, while for non-adiabatic channels $\beta = 2$. For calculations performed with no imposed inlet flow, a quiescent flow is taken initially. For flows with an imposed inlet mass flux, the velocity field is initialized as a Poiseuille flow of strength u_c throughout the channel. A constant-pressure gradient based on u_c is used to describe the initial pressure distribution. Steady-state propagation is assumed

to exist when the rate of change of reaction rate in time has decreased below some threshold value. The constant-density solutions used for comparison with the variable-density cases are obtained by the numerical solution of (2.1*d*,*e*) with $\rho = 1$, $u = u_c(2y - y^2)$ and $v = 0$. Such solutions have been obtained previously by Daou & Matalon (2001, 2002), Liu (2003) and Kessler (2006).

For the figures below, the following parameters have been chosen (unless noted otherwise): $L = 100$, $Q = 2.5$, $\theta = 25$, $Pr = 1$, $Le = 1$ and $D = 7.481 \times 10^3$. Variations in the Péclet number Pe ($= Re$ when $Pr = 1$) result from changes in the half-channel height $\tilde{a}$ and are chosen in the range $Pe \leqslant O(1)$. Since the Péclet number is proportional to the ratio of the half-channel height over the laminar flame thickness, we are only concerned here with thick or moderately thick flames.

4.2. *Adiabatic channels*

4.2.1. *Semi-closed tube; propagation from closed to open end*

The first case we examine concerns the dynamics of a flame in a semi-closed adiabatic ($k = 0$) channel propagating from the closed end ($x = L$) to the end ($x = 0$) open to the atmosphere, i.e. with boundary conditions (2.7) at $x = 0$ and (2.8) at $x = L$. Here $L = 50$. The initial hotspot was placed at the endwall with $x_0 = L$.

Figure 2(*a*) shows the burning rate Ω as a function of the Péclet number Pe once the flame has reached a steadily propagating state. Figure 2(*b*) shows the corresponding magnitude of the induced axial velocity u_i downstream of the flame at $x = 0$, $y = 1$, an outflow that occurs due to thermal expansion in the channel in order for the axial velocity to relax to $u = 0$ downstream of the flame. Figure 2(*c*) shows the corresponding axial propagation speed U of the steady flame. For small Péclet numbers the burning rate limits to one, while the magnitude of the axial velocity on $y = 1$ limits to -3.75 ($= -3Q/2$ for $Q = 2.5$) at $x = 0$, as predicted by the $Pe \to 0$ analysis shown in § 3. Likewise, the axial flame propagation velocity U limits to 3.5 ($U = 1 - 2u_i/3$) as $Pe \to 0$. As the Péclet number increases, the burning rate increases, with a concomitant rise in the magnitudes of u_i and U. In particular, the burning rate remains close to one for $Pe \leqslant 1.8$, with u_i remaining close to $-3Q/2$ and U close to $1 - 2u_i/3$. Beyond $Pe \approx 1.8$, the rise in Ω, u_i and U is significantly more rapid. A little beyond $Pe = 3.6$, steadily propagating solutions cease to exist.

Figure 3 shows the flame structure as a set of mass fraction contours, the velocity vector field, and the axial and transverse velocity variations in the region of the flame zone after it reaches the steady propagation phase for the small Péclet number $Pe = 0.37425$. The basic nature of the $Pe \to 0$ flow analysed in § 3 is revealed. Upstream of the flame, a flow in the direction of the channel exit $x = 0$ has been induced. Examination of the axial and transverse velocity contours reveals the upstream flow to be of an apparent unidirectional Poiseuille form, that attains a constant magnitude shortly upstream of the flame zone (figure 3*a*,*b*). A tranverse velocity variation is present only within the flame zone, having a magnitude smaller than that characterizing the axial velocity (figure 3*c*). This description is consistent with the $O(Pe)$ magnitude of v as $Pe \to 0$ (§ 3). The separable nature of the axial flow variation predicted in § 3 for small Péclet numbers is verified in figure 4(*a*). Plotted is the quantity $u/(2y - y^2)$ from figure 3(*b*), corresponding to $\tilde{u}_0(\xi)$ in § 3, along $y = 1$. Plots of $u/(2y - y^2)$ along $y = 3/4$, $y = 1/2$ and $y = 1/4$ overlay those shown. Moreover, the graph of $u/(2y - y^2)$ is overlaid by the small-Péclet-number solution (3.30) with $u_c = -3Q/2$, where T_0 is obtained by numerical solution of the planar laminar flame equations (3.23) and (3.25). Similarly, the variation of $\partial p/\partial x$ along $y = 1$ obtained from the calculation in figure 3 is shown in figure 4(*b*). Also shown is

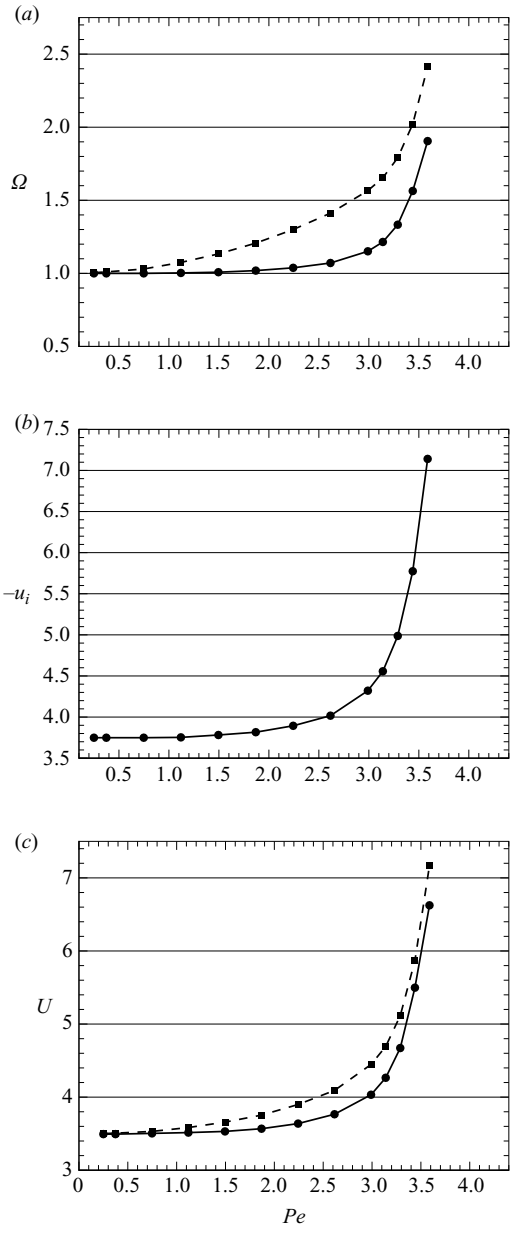

FIGURE 2. (*a*) Burning rate Ω against Péclet number Pe for a flame propagating away from the closed end of a channel towards the open end. (*b*) Corresponding magnitude of induced axial flow velocity on $y = 1$ at the exit plane. (*c*) Corresponding axial flame propagation speed. In (*a*) and (*c*), the dashed lines represent the results obtained from a CDM.

the leading-order $Pe \to 0$ pressure-gradient solution (3.11). Finally, the variation of v along $y = 1$ shown in figure 4(*c*) is close to the $O(Pe)$ expression (3.18).

Figure 5(*a*) shows the flame structure and velocity field vectors during steady propagation for $Pe = 2.994$. With a larger Péclet number (associated with a wider channel), the upstream induced flow causes the flame zone to deform so that it is convex in the upstream direction. Consequently, the increase in flame surface area

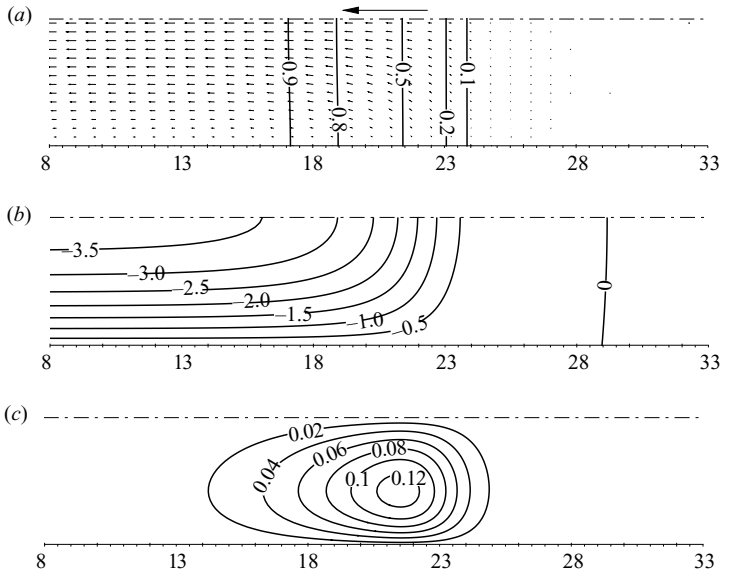

FIGURE 3. (*a*) Fuel mass fraction contours (with the solid lines representing $Y = 0.9$, 0.8, 0.5, 0.2 and 0.1) overlaid with velocity field vectors for a flame propagating from the closed to the open end of a channel with $Pe = 0.37425$ at $t = 14.37$. (*b*) Corresponding axial velocity variation (u). (*c*) Corresponding transverse velocity variation (v).

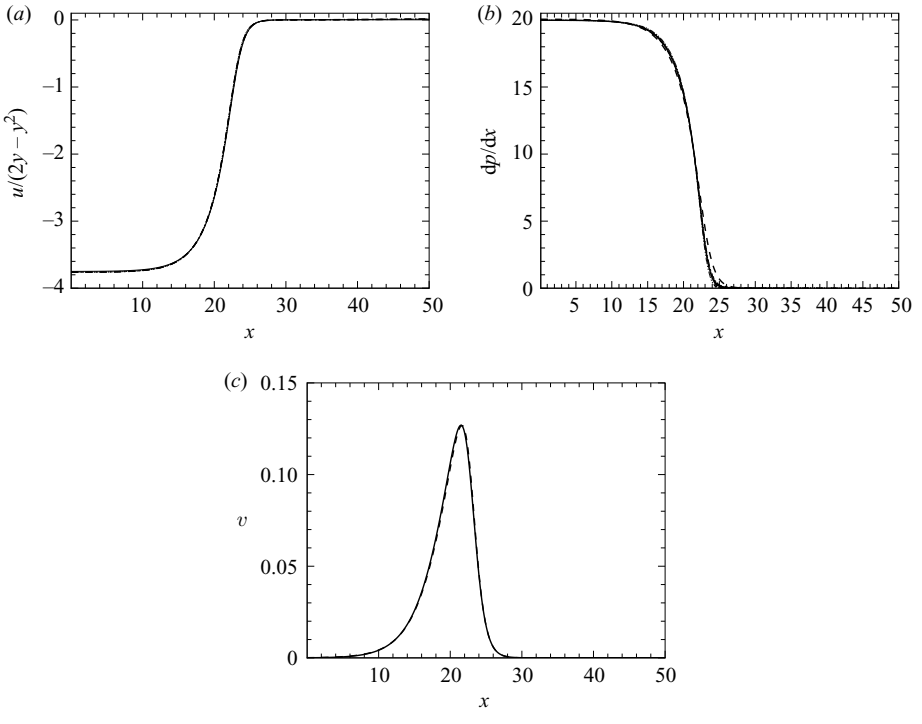

FIGURE 4. Variation of (*a*) $u/(2y - y^2)$, (*b*) $\partial p/\partial x$ and (*c*) v with axial coordinate x along $y = 1$ for the calculation shown in figure 3 ($Pe = 0.37425$). In (*a*) and (*b*), similar plots along $y = 3/4$, $y = 1/2$ and $y = 1/4$ overlay those shown. Also shown in (*a*), (*b*) and (*c*) as the dashed lines are the equivalent variations calculated from the $Pe \to 0$ solution in § 3.

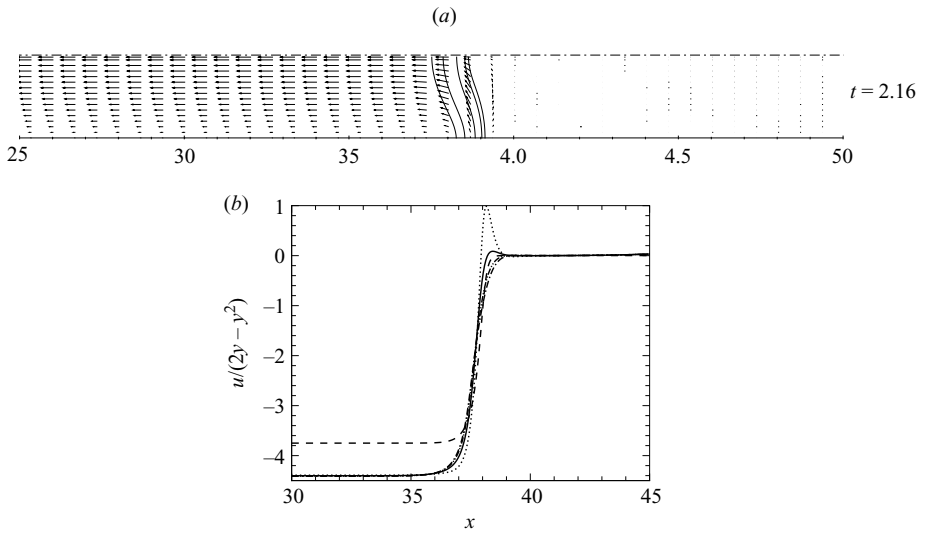

FIGURE 5. (*a*) Fuel mass fraction contours (with the solid lines representing $Y = 0.9$, $Y = 0.8$, $Y = 0.5$, $Y = 0.2$ and $Y = 0.1$) overlaid with velocity vectors for a steadily propagating flame travelling from the closed to the open end of a channel with $Pe = 2.994$ at the indicated time. (*b*) Variation of $u/(2y - y^2)$ with axial coordinate x along $y = 1$ (dash-dotted line), $y = 3/4$ (dash-dot-dotted line), $y = 1/2$ (solid line) and $y = 1/4$ (dotted line) for the calculation shown in (*a*). The $Pe \to 0$ solution is given by the dashed line.

results in an increase in the burning rate above that of the planar laminar flame value of one. The nature of the induced flow upstream still retains a Poiseuille character, as illustrated in figure 5(*b*), except now the increase in burning rate results in an increase in the magnitude of the induced flow over $u_i = -3Q/2$. Shown in figure 5(*b*) is the quantity $u/(2y - y^2)$ evaluated at $y = 1$, $3/4$, $1/2$ and $1/4$. The axial flame propagation speed has also increased above the $Pe \to 0$ prediction of $U_0 = 1 - 2u_i/3 = 3.5$. Outside of the flame zone, the curves of $u/(2y - y^2)$ are nearly coincident. For this case, $\Omega = 1.150$, $u_i = -4.32$ and $U = 4.025$.

Returning now to figure 2, also shown in (*a*) and (*c*) are the burning rate and axial flame speed predictions from a constant-density calculation. In the CDM, combustion does not influence the flow field. Thus a constant-density solution with no imposed flow in the adiabatic channel, that matches the endwall condition of $u = 0$, will result in a uniform burning rate of one for all Péclet numbers. The constant-density results shown in figure 2 are therefore obtained through the insight given by the small-Péclet-number analysis in § 3. In the $Pe \to 0$ limit, the axial speed of a flame propagating away from a closed wall in a VDM will match that obtained through a CDM provided a flow of magnitude $u = -3Q(2y - y^2)/2$ is imposed in the constant-density calculation. The magnitude of this assisted axial flow corresponds to the magnitude of the outflow characterized by $u_i = -3Q/2$ that is induced in the variable-density calculation. Based on this, the constant-density calculations shown in figure 2 are calculated in the following way. Equations (2.1*d*,*e*) are solved numerically with $\rho = 1$, $u = u_i(2y - y^2)$ and $v = 0$, using the same Péclet and Damköhler numbers as in the variable-density case, and with u_i chosen to match the magnitude of the centreline outflow u_i calculated from the variable density case (obtained from figure 2*b*). Calculated in this manner, the burning rate and the axial flame propagation speed variation with Péclet number observed in figures 2(*a*,*c*) have the same qualitative variation as the variable-density

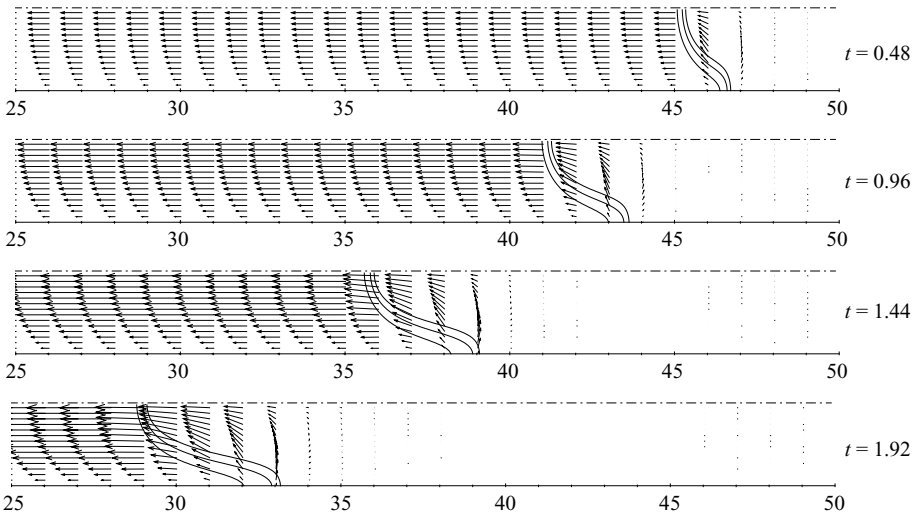

FIGURE 6. Fuel mass fraction contours (solid lines) overlaid with velocity field vectors for an accelerating flame (propagating from $x = L$ to $x = 0$) with $Pe = 5.988$ at several shown time instants. Fuel mass fraction contour levels are 0.8, 0.5 and 0.2.

predictions but with both Ω and U calculated from the CDM overpredicting those from the VDM calculation. Insights into the reason for this are given by the discussion in § 3 on the relative deformations experienced by surfaces of constant-mass fraction between the VDM and the CDM. As noted in § 3, for $u_i = -3Q/2$, the magnitude of the mass flux $\rho_0 \tilde{u}_0$ decreases through the flame zone in the VDM, so that in turn the $O(Pe^2)$ flow-induced spatial deformation of each surface of constant-mass fraction decreases through the flame zone. For the CDM, the spatial deformation of each such surface is constant and equal to the deformation at the head of the flame in the VDM. Consequently, it should be expected that the CDM will predict a higher burning rate and a larger axial flame propagation speed. Nevertheless, calculations conducted with the CDM in the above manner lead to qualitatively better predictions of the VDM behaviour in Ω and U than CDMs calculated with no imposed flow.

As noted above, when the Péclet number is increased beyond that shown in figure 2, steadily propagating flame solutions cease to exist for the initial hotspot conditions described in § 4.1. (We have not studied how the Péclet number boundary between steady and unsteady solutions may be affected by the initial condition form.) Figure 6 shows snapshots of the flame front and the thermal-expansion-induced velocity field vectors for $Pe = 5.988$ at several time instants. The solution does not evolve to a steady one, but rather the flame undergoes a smooth acceleration along the channel. For this calculation, the induced axial velocity variation upstream of the flame zone can still be fitted by a Poiseuille flow profile to a good approximation, but with the intensity of the upstream induced flow increasing in time, as is clearly evident from figure 6. Calculations conducted in longer adiabatic channels do not affect this outcome. Corresponding to the increase in the magnitude of the induced flow, the flame is continually deformed, developing greater surface area as it propagates down the channel. Such accelerating flames, a consequence of thermal-expansion-induced flow by a confined variable-density flame, have been previously observed by Liu (2003) and Ott *et al.* (2003) in a narrow adiabatic channel configuration. In our case, and that of Liu (2003), the induced flow is of a Poiseuille type, rather than the wall

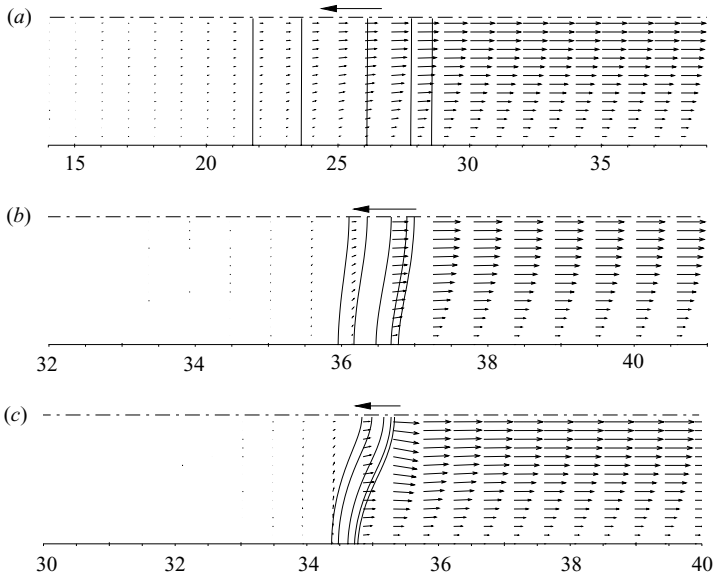

FIGURE 7. Fuel mass fraction contours (solid lines, with $Y = 0.9,\ 0.8,\ 0.5, 0.2$ and 0.1) overlaid on the velocity field vectors for steady-flame propagation towards the closed end of the channel with (*a*) $Pe = 0.37425$, (*b*) $Pe = 2.994$ and (*c*) $Pe = 5.988$.

boundary layer flow observed by Ott *et al.* (2003). Such accelerating solutions may be expected to exist for a finite range of Péclet numbers in which channel confinement and thermal expansion are sufficient to sustain the flame deformation. In summary, for propagation away from the closed end of a channel, thermal expansion induces a flow upstream of the flame zone towards the channel exit in order to relax the axial velocity to the closed endwall conditions downstream of the flame zone. For small Péclet numbers, the induced flow is of the Poiseuille type, but the curvature of the induced flow only influences the flame shape at $O(Pe^2)$. For higher Péclet numbers, the flame zone deforms under the influence of the thermal-expansion-induced flow.

4.2.2. *Propagation in a semi-closed channel; towards the closed end*

Figure 7 shows the flame structure and induced flow for a steady flame propagating towards the closed end ($x = 0$) of a semi-closed adiabatic channel for $Pe = 0.37435$, $Pe = 2.994$ and $Pe = 5.988$. The channel is open at $x = L$, where $L = 100$. Thus boundary conditions (2.8) are applied at $x = 0$ and (2.7) at $x = L$. The initial hotspot was placed at the channel centre with $x_0 = L/2$. Consequently, two oppositely propagating flames are observed; the results shown below are subsequent to the transient downstream-moving flame being blown out of the channel. As the observed flame propagates towards the closed endwall, thermal expansion induces a flow downstream of the flame in a direction towards $x = L$. Correspondingly, the flame becomes concave towards the direction of propagation. For small Péclet numbers, the flow downstream of the flame is again of the Poiseuille type, where the magnitude of the downstream axial velocity on the centreline is $u_i = 3Q/2$. In figure 7, $\Omega = 1$, $u_b = 3.75$ and $U = 1$ for $Pe = 0.37425$, $\Omega = 1.03$, $u_b = 3.87$ and $U = 1.03$ for $Pe = 2.994$ and $\Omega = 1.18$, $u_b = 4.43$ and $U = 1.17$ for $Pe = 5.988$, where u_b is the magnitude of the downstream axial flow velocity along $y = 1$. Thus, for a given Péclet number, the burning rate is smaller for a flame propagating towards the closed end of the channel

as opposed to the open end. In the limit $Pe \to 0$, this is explained as follows. Equations (3.37) and (3.39) reveal that the $O(Pe^2)$ deformation of a surface of constant mass fraction is proportional to the mass flux quantity $\rho_0 \tilde{u}_0$. For the flame propagating towards an open end, the $Y = 1$ contour at the head of the flame has a deformation proportional to $\rho_0 \tilde{u}_0 = -3Q/2$, while that at the rear of the flame has $\rho_0 \tilde{u} = 0$. On the other hand, for the flame propagating towards the closed end, the $Y = 1$ contour has a deformation corresponding to $\rho_0 \tilde{u} = 0$, but the $Y = 0$ surface has a deformation corresponding to $\rho_0 \tilde{u}_0 = 3Q/2(1+Q)$. Consequently, the flame propagating towards the open end is nominally more highly deformed even though the magnitude of the induced flow at the channel exit is the same in either case. As a final note on this case, for $Pe = 5.988$ and propagation towards the open exit, a continuously accelerating flame solution was found. For propagation towards the closed end for $Pe = 5.988$, steadily propagating solutions are found (figure 7*c*). In fact we have not identified any solutions of accelerating form for propagation towards the closed end of the channel.

4.2.3. *Propagation with imposed inlet mass flux*

The effects of thermal expansion on flame propagation in an open channel with an imposed Poiseuille flow at the channel entrance are now examined. Thus conditions (2.6) are applied at $x = 0$ and (2.7) are applied at $x = L$. In this section, adiabatic sidewalls ($k = 0$) are again considered.

Figure 8(*a*) shows the burning rate Ω as a function of the inlet flow magnitude u_c for $Pe = 1.497$, $Pe = 2.994$ and $Pe = 5.988$. Two significant features of the (Ω, u_c) behaviour need to be highlighted. First, for each of the Péclet numbers considered, the burning rate corresponding to an imposed channel inflow of a given centreline ($y = 1$) magnitude u_c (> 0) is larger than the burning rate for an imposed channel outflow of the same magnitude $-u_c$ (< 0). Second, the burning rate variation for $u_c < 0$ has a minimum at some finite value of u_c for the three Péclet numbers shown (see figure 8*c*). In the limit $Pe \to 0$, the first feature is easily explained, as stated in § 3. In this case, the relative $O(Pe^2)$ deformation of each surface of constant-reactant-mass fraction, proportional to $\rho \tilde{u}_0$, is by virtue of (3.39) larger for an opposed flow with a given $u_c > 0$ than for an assisted flow with magnitude $-u_c$, since $3(1-\rho_0)/2 > 0$. The second property is not easily explained by the extent of the small-Péclet-number analysis conducted in § 3. Indeed, based solely on the analysis of the reactant mass fraction surface deformation behaviour, there is no expectation that in the limit $Pe \to 0$, a flame should develop a minimum in the burning rate at finite u_c (with $u_c < 0$). As detailed in § 3, certainly any decrease in u_c below $-3Q/2$ (for the adiabatic case) should lead to an increase in the burning rate. For $0 > u_c > -3Q/2$, the surfaces of constant-mass fraction at the head of the flame are convex towards the upstream but are concave at the rear of the flame. It is not clear from the $Pe \to 0$ analysis how this outward bulging of the flame affects the burning rate in the regime $0 > u_c > -3Q/2$.

Figure 9 shows various mass fraction contours superimposed on the velocity field vectors for $Pe = 0.37435$ with inlet velocities $u_c = \pm 0.835$. For this small Péclet number, the basic flow and reaction zone structures are similar to those determined in $Pe \to 0$ limit (§ 3). For $u_c = 0.835$ (figure 9*a*), smaller than the blow-off velocity of 3/2, the magnitude of the axial velocity at the outflow boundary $x = L$ is $u_i = 4.58$, while the axial flame propagation speed is $U = 4.40$. The burning rate $\Omega = 1.0001$. Each reactant mass fraction contour is concave to the upstream flow. For $0 > u_c > -3Q/2$ and for $Pe \to 0$, thermal expansion causes the axial flow to reverse direction in the flame zone. Consequently, as noted in § 3, the surfaces of constant mass fraction at the head of the flame are convex towards the upstream but are concave at the rear of

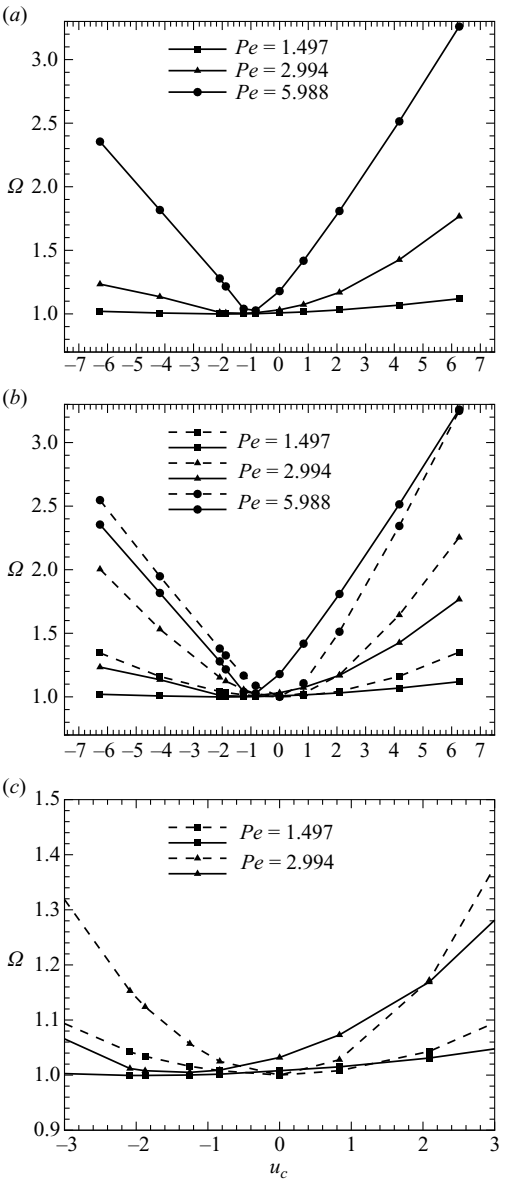

FIGURE 8. Burning rate Ω against the intensity of the prescribed inflow u_c for selected Péclet numbers. The solid lines are based on variable-density simulations. In (b) and (c), the dashed lines represent results obtained from the CDM.

the flame. Figure 9(b) shows the flame structure for $u_c = -0.835$ and $Pe = 0.37435$, a case in which $0 > u_c > -3Q/2$. Then $u_i = 2.93$, $U = 1.54$ and $\Omega = 1.005$. The bulging nature of the flame structure described above is clearly observed in figure 9(c,d), which shows a magnification of the flame structure for the case in figure 9(b).

Figure 10 shows various reactant mass fraction contours superimposed on the velocity vector field for the larger Péclet number $Pe = 5.988$ with inlet velocities $u_c = \pm 0.835$ and $u_c = -4.175$. In this case, the flame thickness is comparable to the channel height. For $u_c = 0.835$ (figure 10a), $\Omega = 1.416$, $u_i = 6.15$ and $U = 0.86$, where

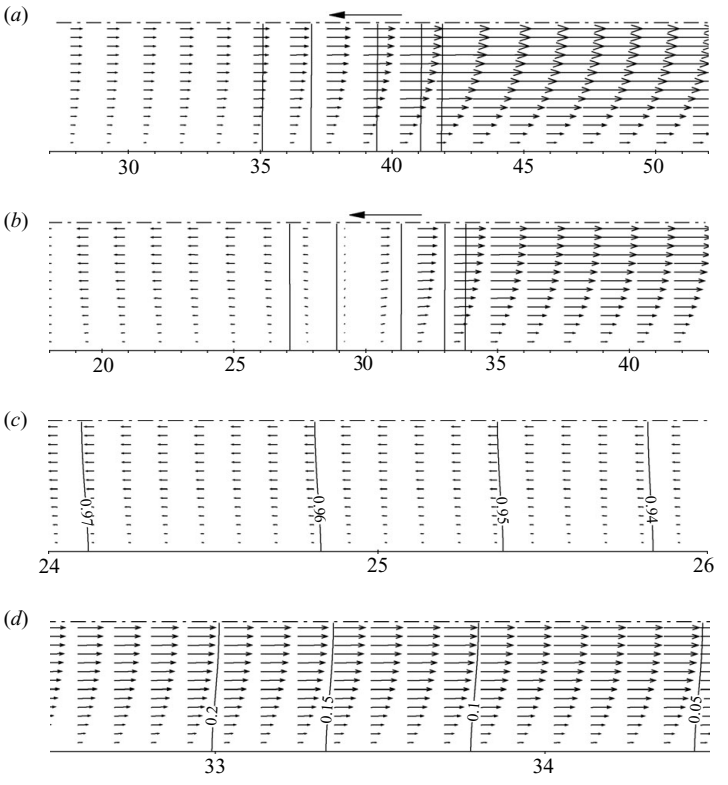

FIGURE 9. Fuel mass fraction (solid lines, for $Y = 0.9$, 0.8, 0.5, 0.2 and 0.1) contours and velocity field vectors for $Pe = 0.37435$ with (*a*) $u_c = 0.835$, (*b*) $u_c = -0.835$. Panels (*c*) (upstream) and (*d*) (downstream) show an expanded view of (*b*) in the vicinity of the flame front.

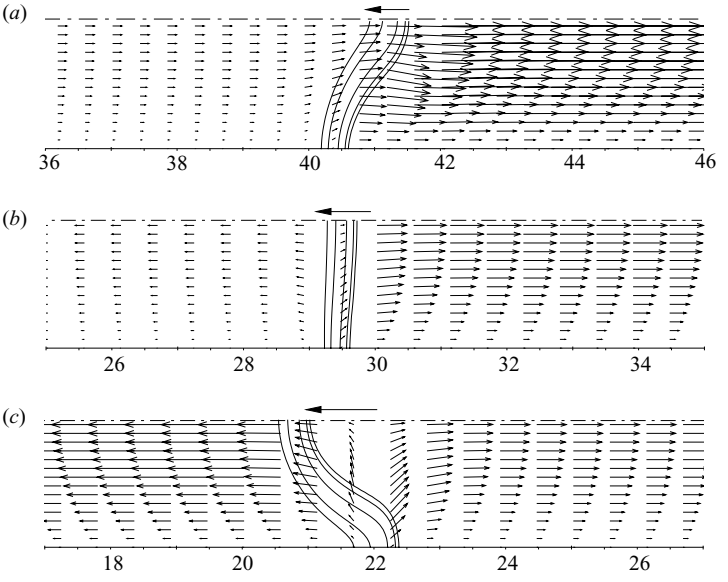

FIGURE 10. Fuel mass fraction contours (solid lines, for $Y = 0.9$, 0.8, 0.5, 0.2 and 0.1) and velocity field vectors for $Pe = 5.988$ with (*a*) $u_c = 0.835$, (*b*) $u_c = -0.835$ and (*c*) $u_c = -4.175$.

the magnitude of the axial flow velocity has increased through the flame zone. The case $u_c = -0.835$ (figure 10*b*) corresponds to a point near where the minimum in the burning rate occurs in figure 8. Here $\Omega = 1.027$, $u_i = 3.04$ and $U = 1.58$. As shown in figure 10(*b*), the flame is approximately planar, hence the attainment of a burning rate close to one (figure 8*a*). The planar structure arises due to the effects of thermal expansion. The imposed channel outflow at the channel entrance attempts to induce a flame curvature such that the flame is convex towards the upstream. Thermal expansion acts to reverse the direction of the flow, attempting to make the flame concave towards the upstream. For $u_c = -0.835$, the net result is a nearly planar flame structure. For $u_c = -4.125$, the flame is convex towards the upstream, with $\Omega = 1.818$, $U = 4.60$ and $u_i = 2.66$. Consequently, the direction of the axial flow downstream of the flame is in the sense which is opposite that of the upstream flow even though $u_c < -3Q/2$. The curvature of the flame observed in this case is sufficient to induce a flow reversal through the flame zone that does not occur in the $Pe \to 0$ limit.

Figure 8(*b*,*c*) shows the comparison between the burning rates obtained in the CDM and the VDM as u_c is varied. In the limit $Pe \to 0$, and based on arguments over how the burning rate should be affected by spatial deformation, it was demonstrated in § 3 that for $u_c > 0$ the burning rate for the VDM should be lower than that of the CDM under blow-off conditions (i.e. for $u_c > 3/2$). For $0 \leqslant u_c < 3/2$, the opposite is true. For $u_c < 0$ and sufficiently small, it was concluded that the VDM should have a higher burning rate but that at some undetermined value of u_c, the CDM should have the higher burning rate. This general behaviour is reproduced in figure 8(*b*,*c*) for the Péclet numbers shown. For $u_c > 0$, an increase in Pe increases the value of u_c at which the VDM and the CDM transition between the higher and lower burning rates. Similarly for $u_c < 0$, the transition point occurs for decreasing u_c. Overall, the CDM does an adequate job of capturing the correct (Ω, u_c) variation.

4.3. *Non-adiabatic channels*

4.3.1. *Semi-closed channel; propagation towards the open or closed end*

We now turn our attention to the effects of density variation and comparisons with the constant-density approximation, for flame propagation in a non-adiabatic channel. In the following, we restrict our attention to small and moderate Péclet numbers for which there exists a κ where complete, rather than partial, quenching is possible in the channel (Daou & Matalon 2002). There are significant differences with flame propagation in adiabatic channels, and these are highlighted below. Flame propagation in a semi-closed channel, with the flame propagating towards either the closed or the open end, is considered initially. In the small-Péclet-number limit $Pe \to 0$, and for a sufficiently long channel (such that the temperature is able to relax to the upstream value downstream of the flame), the steady flow solution is given by (3.23), (3.25) and (3.30) in § 3. Thus, in a sufficiently long channel with no imposed open end flow, the cases of propagation either towards the closed end or towards the open end away from the closed wall are identical. This is in contrast to the adiabatic case, where propagation away from the closed end induces an upstream axial Poiseuille flow in the direction of flame propagation, having a magnitude $\tilde{u}_i = -3Q/2$, while propagation towards the closed end induces a downstream Poiseuille flow opposite to the flame propagation direction, having a magnitude $\tilde{u}_i = 3Q/2$. Also, in the adiabatic case the flame propagating towards the open end has the higher burning rate. For the non-adiabatic problem, in both cases, the axial flow magnitude $\tilde{u}_0$ on $y = 1$ increases from zero upstream in a direction opposed to that of flame propagation, reaches a

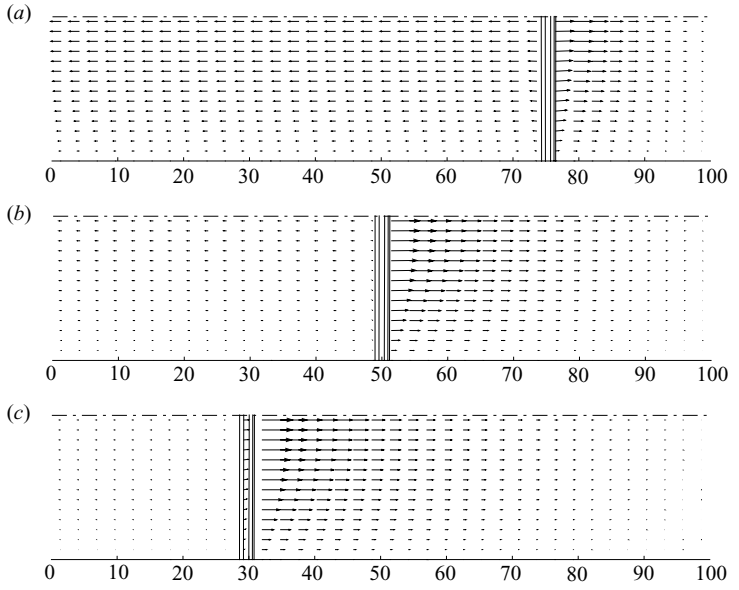

FIGURE 11. Fuel mass fraction contours (solid lines, with $Y = 0.9$, 0.8, 0.5, 0.2 and 0.1) and velocity field vectors for flame propagation away from the closed end of a channel ($x = 100$) with $Pe = 1.497$ and $k = 0.06$ ($\kappa = 0.02677$) at (*a*) $t = 11.98$, (*b*) $t = 35.93$ and (*c*) $t = 59.88$.

maximum when $\tilde{u}_0 = 3M(\max[T_0] - 1)/2$ and then decreases to zero downstream of the flame as heat losses cause T_0 to relax to one.

In practice, the length of the channel required to reach a steady-state solution will depend on the heat loss parameter k. Initially, in finite-length channels, unsteady transients should be expected, as the downstream temperature at the closed or the open end is influenced by heat losses. Figure 11 shows a sequence of snapshots of the evolution in the induced velocity field for a flame propagating from the closed to the open end of a channel for $Pe = 1.497$ and $k = 0.06$ (or $\kappa = k/Pe^2 = 0.02677$). The channel length is $L = 100$, and the flame is initiated at the closed end by a hotspot with $x_0 = L$. During the early stages of the evolution when $T > 1$ at $x = L$, an axial, Poiseuille-like, flow is induced upstream of the flame, as shown in figure 11(*a*). In the limit $Pe \to 0$, and assuming that the time scale of relaxation to the steady solution is large, the instantaneous magnitude of the induced flow upstream would be $u_i = -3M(T_L - 1)/2$, where T_L is the temperature at the closed wall. At $t = 11.976$ (figure 11*a*), the magnitude of the induced axial flow at $x = 0$ and $y = 1$ is $u_i = -0.824$, while the axial propagation speed is $U = 1.32$ and the burning rate is $\Omega = 0.775$. The temperature $T = T_L$ (taken at $x = L$ and $y = 1$) is $T_L = 1.94$. In the $Pe \to 0$ limit, $\Omega = M$ and using the preceding values $-3M(T_L - 1)/2 = -1.09275$, which is larger than the calculated value $u_i = -0.824$. On the other hand, in the small-Péclet-number limit, the axial velocity U is $M - 2u_i/3$. Using the preceding values, $M - 2u_i/3 = 1.3243$, close to the calculated value. In figure 11(*a*), thermal expansion causes the axial flow direction to reverse through the flame. The magnitude of the reversed flow falls in the region between the flame and the endwall, as heat losses lead to a drop in temperature downstream of the flame, limiting the local thermal expansion. As time progresses, the temperature at the endwall drops, and thus the magnitude of the induced flow out of the channel must also decrease (cf. (3.30)). In figure 11(*b*), $u_i = -0.224$, $U = 0.92$, $\Omega = 0.762$ and $T_L = 1.27$ ($-3M(T_L - 1)/2 = 0.3086$,

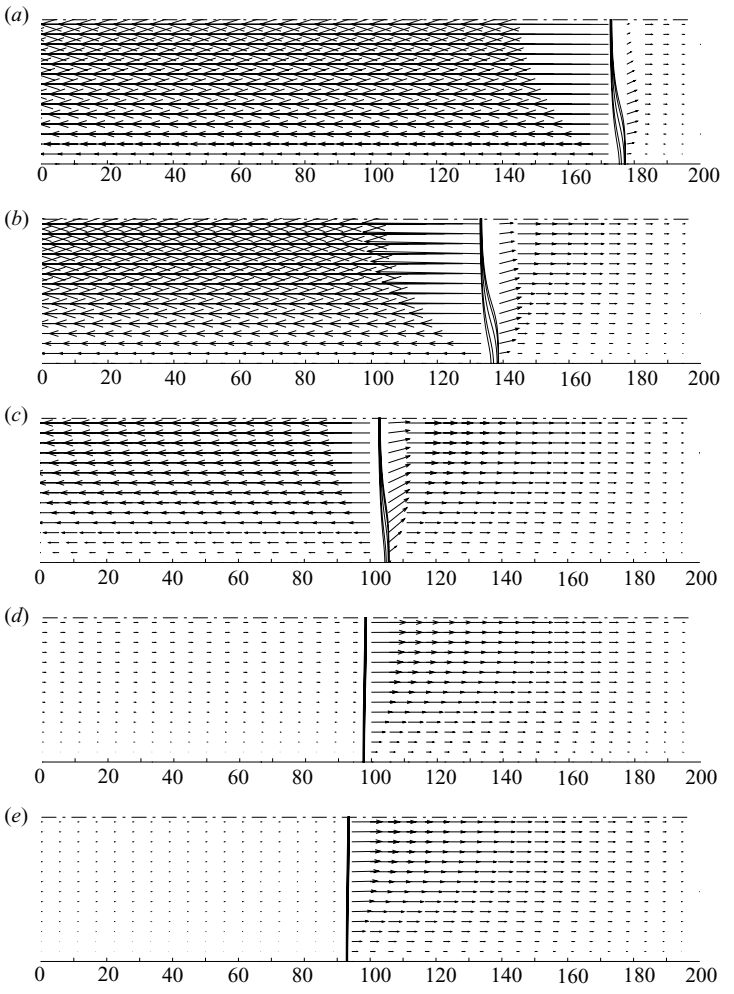

FIGURE 12. Fuel mass fraction contours (solid lines, with $Y = 0.9$, 0.8, 0.5, 0.2 and 0.1) and velocity field vectors for flame propagation away from the closed end of a tube with $Pe = 5.988$ and $k = 0.1$ ($\kappa = 0.002789$) at (*a*) $t = 2.3952$, (*b*) $t = 4.7904$, (*c*) $t = 7.1856$, (*d*) $t = 9.5808$ and (*e*) $t = 14.3712$.

$M - 2u_i/3 = 0.911$), while in figure 11(*c*), $u_i = -0.078$, $U = 0.77$, $\Omega = 0.758$ and $T_L = 1.10$ ($-3M(T_L - 1)/2 = 0.1137$, $M - 2u_i/3 = 0.81$). In figure 11(*c*), the spatial deformation of each surface of constant-mass fraction is concave to the upstream direction. Thus, even though the effect of heat loss is to induce a deformation in the flame shape to be convex in the direction of propagation, for moderately small Péclet numbers, the spatial deformation of each surface of constant-mass fraction is dominated by thermal expansion (as shown in (3.39)).

Figure 12 shows the evolution of the velocity field for $Pe = 5.988$ and $k = 0.1$ (or $\kappa = 0.002789$). In an adiabatic channel continuously accelerating flames were identified for this Péclet number (figure 6). Initially, while the temperature on the endwall has yet to be substantially influenced by heat loss, accelerating flames are also identified in figure 12 in combination with a significant induced upstream axial flow. The strong axial flow induces a significant deformation of the flame towards the

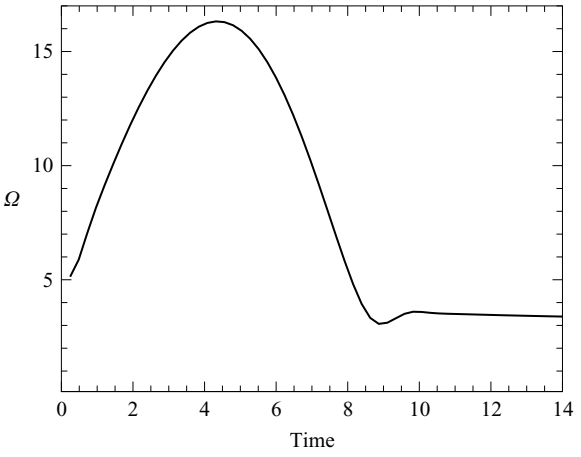

FIGURE 13. Burning rate against time for figure 12.

upstream. In figure 12(*a*), $u_i = -14.97$, $U = 14.8$, $\Omega = 4.43$ and $T_L = 3.82$, while in figure 12(*b*), $u_i = -16.98$, $U = 16.7$, $\Omega = 5.40$ and $T_L = 3.35$. As the temperature at the endwall drops, figure 12(*c*) (where $T_L = 3.04$) shows a drop in the magnitude of the induced upstream flow, where $u_i = -7.21$ and a corresponding drop in the axial flame propagation speed ($U = 7.4$) and the burning rate ($\Omega = 3.08$). In figure 12(*d*, *e*), the magnitude of the induced upstream flow drops further, and a further decay in the burning rate occurs, as shown in figure 13. In figure 12(*e*), $u_i = 0.12$, $U = 0.95$, $\Omega = 1.13$ and $T_L = 2.45$. Note, in addition, the relative flatness of the flame in figure 12(*d*, *e*), despite the relatively large Péclet number, as the flame approaches a propagation phase in which changes in the burning rate occur on a slower time scale as T_L relaxes to one. The flatness results from a balance between heat loss, which causes a spatial deformation of the flame convex to the upstream direction, and the local thermal-expansion-induced axial flow field, which induces a spatial deformation of the flame concave to the upstream direction. In addition to the present study, Ott *et al.* (2003) also found that accelerating flames could not be found in non-adiabatic channels. Here the reason for this is identified as the decay of the thermal-expansion-induced flow upstream of the flame due to the heat loss limiting of thermal expansion downstream of the flame, so that the influence of thermal expansion becomes localized around the flame zone region. Thus accelerating flames only appear to exist as transient solutions in sufficiently long non-adiabatic channels (as in figure 12).

Figure 14 shows the burning rate obtained by a steadily propagating flame as a function of the heat loss parameter $\kappa = (k/Pe^2)$ for a flame propagating towards the closed channel wall with $Pe = 0.7485$, $Pe = 1.497$ and $Pe = 2.994$. In these calculations, for each κ, the channel length L is taken to be sufficiently long for the burning rate to relax to a steady value where $T_L \to 1$ downstream of the flame. The variation in the curves for $Pe = 0.7485$ and $Pe = 1.497$ is small. For $Pe = 2.994$ and small values of the heat loss parameter κ, the burning rate is larger than for $Pe = 1.497$ and $Pe = 0.7485$. For larger values of κ, where the burning rate is more substantially affected by the heat loss, the calculated burning rate for $Pe = 2.994$ is close to those for $Pe = 1.497$ and $Pe = 0.7485$. For each fixed Pe, the critical value of κ_c, where for $\kappa > \kappa_c$ quenching occurs, are similar, where $\kappa_c \approx 0.035$. This is in excellent agreement with the value of $\kappa_c \approx 0.036$ obtained from the small-Péclet-number large-activation energy result (3.27).

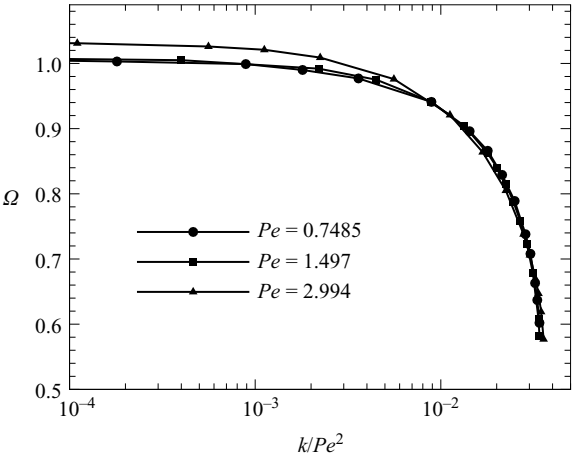

FIGURE 14. Burning rate Ω as a function of k/Pe^2 for flame propagation towards the closed end of the channel. Péclet numbers are as shown.

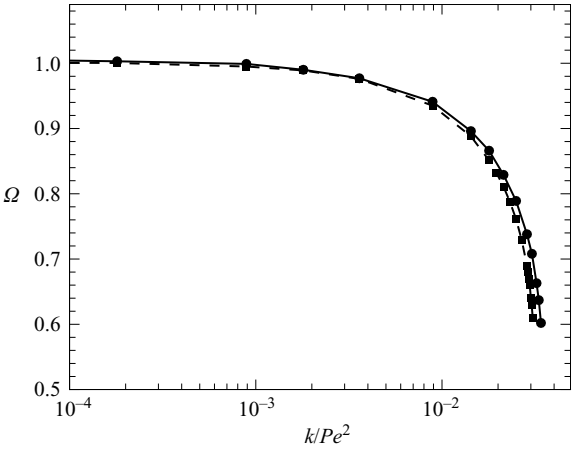

FIGURE 15. Comparison of the burning rate Ω as a function of k/Pe^2 for flame propagation towards the closed end of the channel for the VDM (solid line) and the CDM (dashed line) for $Pe = 0.7485$.

An examination of the flame structures near the quenching region for these three Péclet numbers shows the flames to be approximately one-dimensional, resulting from the opposing flame deformation effects of heat loss and thermal expansion. Figure 15 shows a comparison of the burning rate Ω as a function of κ between the VDM and the CDM for the $Pe = 0.7485$ case shown in figure 14. The curves are quantitatively similar, a result of the similar nature of the $Pe \to 0$ VDM and CDM given by (3.23) and (3.25). However, the CDM gives a lower value of κ_c ($= 0.0307$).

4.3.2. *Propagation with an imposed inlet Poiseuille flow*

Figure 16 shows the variation of the burning rate with centreline inlet velocity u_c for $k = 0.15$ ($\kappa = 0.01673$) and $Pe = 2.994$ for the VDM. Of most interest is that for this Péclet number, the burning rate Ω is larger for a flame-assisted flow ($u_c < 0$) than for a flame-opposed flow of the same magnitude. The difference between assisted and opposed flow burning rates increases as the magnitude of u_c increases. The opposite

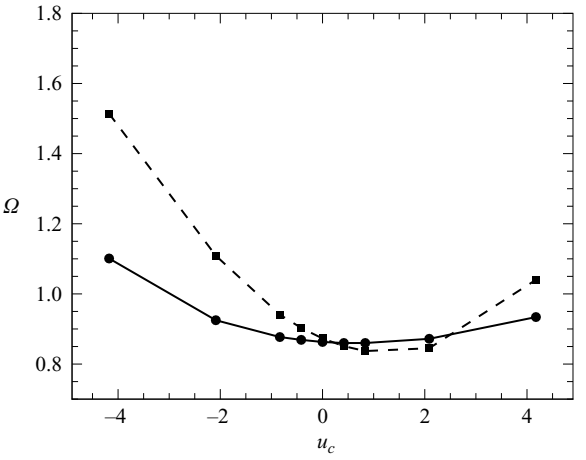

FIGURE 16. Comparison of the burning rate Ω against the intensity of the prescribed inflow u_c for $Pe = 2.994$ and $k = 0.15$ ($\kappa = 0.01673$) for the variable-density (solid line) and constant-density (dashed line) simulations.

has been found for flame propagation in an adiabatic channel for $Pe = 2.994$ (figure 8) and in the small-Péclet-number limit. The $Pe \to 0$ study in § 3 shows that the relative deformation experienced by a flame opposed by a flow of magnitude u_c (> 0) is greater than that for a flame assisted by a flow of the same magnitude u_c (< 0) regardless of the heat loss κ. The heat loss simply affects the relative magnitudes of the deformation via the value of the flux M in (3.30). In figure 16, for $u_c < 0$, the sidewall heat loss results in a deformation of the flame that occurs in the same direction as that due to thermal expansion, i.e. convex to the upstream. This deformation combination results in a burning rate that is larger than that due to heat loss and thermal expansion for the same magnitude of u_c but with $u_c > 0$. In the $u_c > 0$ case, the deformation due to heat loss (convex to the upstream) occurs in the sense which is opposite that of thermal expansion (concave to the upstream). Based on the $Pe \to 0$ behaviour and figure 16, heat loss plays a more significant role in the determination of relative opposed and assisted burning rates as the Péclet number and the magnitude of u_c increase. The variable-density burning rate curve also has a minimum in the region $u_c > 0$ rather than for $u_c < 0$ as found in the adiabatic channel. Presumably this occurs when the opposing deformation effects of heat loss and thermal expansion for $u_c > 0$ combine to produce the least deformed flame surface. Figure 16 also shows the burning rate variation with u_c obtained from the CDM (Daou & Matalon 2002). The constant-density burning rate for $u_c < 0$ and for sufficiently large $u_c > 0$ is greater than the variable-density burning rate. There is a range of u_c in which $u_c > 0$ for which the constant-density burning rate is smaller than the variable-density burning rate.

Figure 17 shows a comparison of the variation in steady burning rates with heat loss κ from the VDM and the CDM for $Pe = 2.994$ and $u_c = \pm 0.835$. For the flame-opposed case, the agreement between the two model predictions becomes better as κ increases, with reasonable agreement as the heat losses begin to significantly affect the burning rate. For the flame-assisted case, the agreement is poorer in the κ region near the flame-quenching limit. The quenching heat loss parameter κ_c for $u_c = -0.835$ is lower in the VDM ($\kappa_c = 0.0406$) than in the CDM ($\kappa_c = 0.0489$), while for $u_c = 0.835$, $\kappa_c = 0.031$ for the VDM and $\kappa_c = 0.028$ for the CDM. Figure 18 shows

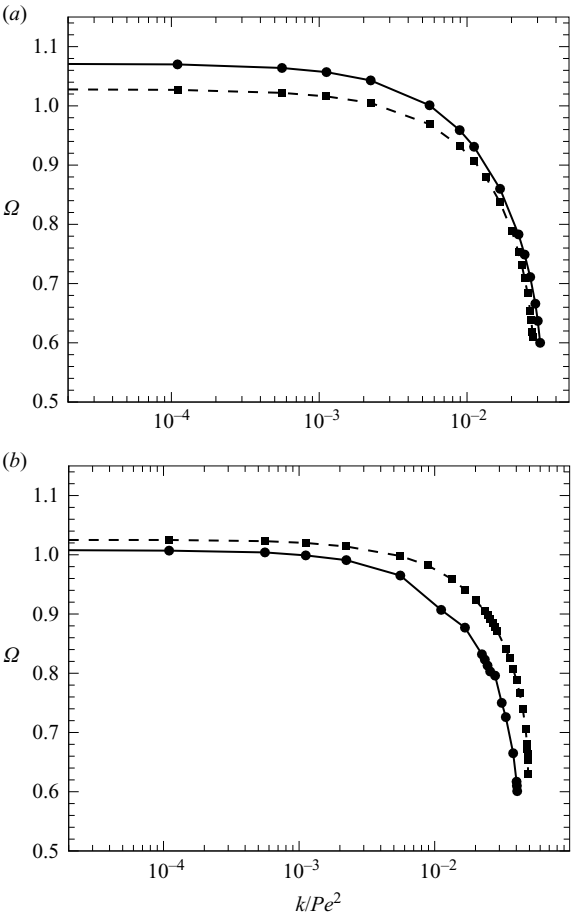

FIGURE 17. Comparison of the burning rate Ω as a function of k/Pe^2 for $Pe = 2.994$ and (*a*) $u_c = 0.835$ and (*b*) $u_c = -0.835$ for the VDM (solid line) and the CDM (dashed line).

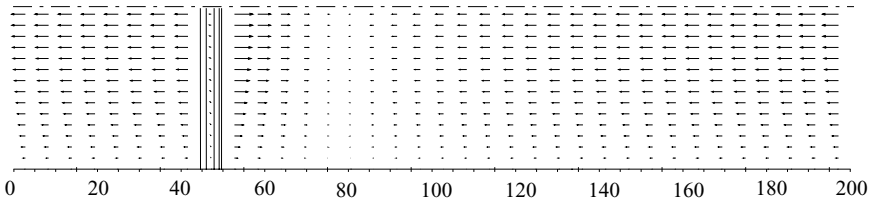

FIGURE 18. Fuel mass fraction contours (solid lines) for $Y = 0.9$, 0.8, 0.5, 0.2 and 0.1 and velocity field vectors for $Pe = 0.7485$ with $u_c = -0.835$ and $k = 0.018$ ($\kappa = 0.03213$).

lines of constant-mass fraction with velocity field vectors for $Pe = 0.7485$, $u_c = -0.835$ and $k = 0.018$ ($\kappa = 0.03213$). As predicted in § 3, thermal expansion causes the axial flow field to reverse direction through the flame, which then decreases in magnitude due to heat loss. Sufficiently far downstream of the flame, the flow reverses direction again, limiting close to $u_c = -0.835$. At the time shown in figure 18, $u_i = 0.902$. Figure 19 shows the deformation of the flame surface for the case shown in figure 18. At the head of the flame, the lines of constant-mass fraction are convex to the upstream, while the rear section of the flame has lines of constant mass fraction

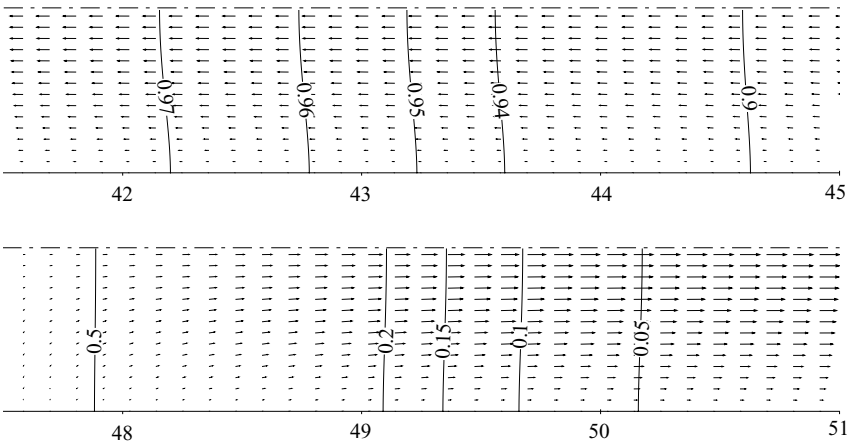

FIGURE 19. Fuel mass fraction contours (solid lines) and velocity field vectors in the vicinity of the flame front for $Pe = 0.7485$ with $u_c = -0.835$ and $k = 0.018$ ($\kappa = 0.03213$).

that are concave to the upstream. Since the reversal in the flow direction shown in figure 18 only occurs far downstream, an additional change in the convexity of the surfaces of constant-mass fraction, a possibility raised in § 3, does not occur.

5. Summary

The influence of thermal expansion on the dynamics of thick to moderately thick premixed flames (flame thickness less than or comparable to the channel height) for a variable-density flow in a narrow, rectangular channel has been examined. This paper extends in those regimes the study of Daou & Matalon (2001, 2002), who considered a constant-density formulation.

The study was conducted within the framework of the zero-Mach-number, variable-density Navier–Stokes equations. Both adiabatic and non-adiabatic channel walls were considered. A small-Péclet-number asymptotic solution was developed for steady variable-density flame propagation in the narrow channel. In this limit, the variations in temperature and species concentrations are governed by the one-dimensional laminar flame solution with a volumetric heat loss term. When written in terms of the mass flux, the equations governing the temperature and concentration variations were identical in form to those derived via a CDM (Daou & Matalon 2002). Quenched solutions are identified within a regime in which the convective heat loss parameter is $O(Pe^2)$, as in Daou & Matalon (2002). The axial velocity is governed by a separable solution consisting of a channel Poiseuille flow with an amplitude modified by thermal expansion. The small-Péclet-number solution was examined for configurations including flame propagation from the closed to the open end of the channel, towards the closed end of the channel and towards the channel inlet with an imposed Poiseuille flow (flame assisting or flame opposing). The quantitative nature of the axial velocity variation, in all cases of Poiseuille form, was dependent on the configuration studied. The burning rate modification of the leading-order small-Péclet-number laminar flame solution due to thermal expansion was examined by calculating the $O(Pe^2)$ spatial deformation experienced by curves of constant-mass fraction. Thermal expansion in a channel with an imposed Poiseuille flow of magnitude $|u_c|$ at the channel entrance causes a flow-opposed flame ($u_c > 0$) to burn at a higher rate than a flow-assisted flame ($u_c < 0$).

The dynamics of narrow-channel flames were also examined numerically for finite Péclet numbers in the configurations mentioned above. Comparisons of the finite-Péclet-number dynamics were made with the predictions of the small-Péclet-number solutions. We also compared how thermal expansion modifies the flow dynamics from those determined from similar studies undertaken in a CDM (Daou & Matalon 2001, 2002). For an adiabatic channel, and for flame propagation away from a closed wall, steadily propagating solutions were identified for sufficiently small Péclet numbers. Thermal expansion through the flame in the confined channel induces a Poiseuille axial flow upstream. The magnitude of the upstream axial flow at the channel exit and the burning rate both increased with increasing Péclet number. In channels of a finite size, continuously accelerating flames occur as a result of thermal-expansion-induced upstream flow and the stretching of the flame surface due to the induced flow, as previously found by Liu (2003) and Ott *et al.* (2003). CDM calculations based on a Poiseuille flow having a magnitude equal to the induced velocity outflow from the variable-density calculations offered a reasonable comparison with the variable-density results. For flame propagation towards the closed end of the channel, the burning rate was smaller, and the induced flow caused a flame deformation in the opposite sense (concave to the upstream), than flames propagating away from the closed end with the same Péclet number. No accelerating flames were identified in this case. For finite Péclet numbers, the burning rate variation for an imposed channel inlet flow of magnitude u_c continued the $Pe \to 0$ limit behaviour of having a larger value for flame-opposed flows. In non-adiabatic channels, in the case of flame propagation towards the open end of the channel, accelerating flames were only identified as transient solutions, before the onset of steadily propagating flames. Here, heat loss minimizes the role of thermal expansion upstream and downstream of the flame, localizing the effects of thermal expansion to the flame zone region. Also, as the Péclet number increases, heat loss can result in the burning rate of a flow-assisted flame to become greater than that of a flow-opposed flame, where the flow magnitude is the same in both cases. When plotted as a function of $\kappa = k/Pe^2$, the heat loss parameter κ for complete quenching was similar for different Péclet numbers for the variable-density calculations (Daou & Matalon 2002). The small-Péclet-number variable-density solution for a flame propagating in a circular pipe is also given in an appendix.

DAK was funded by the Air Force Office of Scientific Research, the Center for the Simulation of Advanced Rockets at the University of Illinois and the Naval Research Laboratory through the Office of Naval Research. MS was supported by the Department of Energy. The authors are also grateful to Professor Moshe Matalon, Dr Elaine Oran and Dr Vadim Gamezo for many engaging discussions during the preparation of this manuscript.

Appendix. $Pe \to 0$ analysis for circular pipe flow

Here we derive the solution for symmetric variable-density flame propagation in a circular pipe the radius of which is smaller than the flame thickness. The radial and axial coordinates are denoted by r and z respectively, while the axial velocity is u_z and the radial velocity is u_r. Along $r = 0$, the symmetry conditions

$$\frac{\partial T}{\partial r} = 0, \quad \frac{\partial Y}{\partial r} = 0, \quad \frac{\partial u_z}{\partial r} = 0, \quad u_r = 0, \quad \frac{\partial p}{\partial r} = 0 \qquad \text{(A 1}a\text{–}d\text{)}$$

are applied, while along $r = 1$ the conditions

$$\frac{\partial T}{\partial r} = -Pe^2\kappa(T-1), \quad \frac{\partial Y}{\partial r} = 0, \quad u_z = 0, \quad u_r = 0 \tag{A 2a–d}$$

hold. For an imposed Hagen–Poiseuille flow at $z = 0$ with an open pipe at $z = L$, the conditions

$$T = 1, \quad Y = 1, \quad u_z = u_c(1-r^2), \quad u_r = 0 \tag{A 3a–d}$$

are applied at $z = 0$, while the conditions

$$\frac{\partial T}{\partial z} = 0, \quad \frac{\partial Y}{\partial z} = 0, \quad \frac{\partial u_z}{\partial z} = 0, \quad \frac{\partial u_r}{\partial z} = 0, \quad p = 0 \tag{A 4}$$

are applied at $x = L$. As in § 3, the flame propagates to the left (z decreasing) with constant axial velocity U. With the scalings adopted in § 3, $\xi = Pe(z + Ut)$ and $\bar{p} = Pe^2 p$, (2.1) becomes

$$Pe\frac{\partial}{\partial \xi}(\rho(u_z + U)) + \frac{1}{r}\frac{\partial}{\partial r}(\rho r u_r) = 0, \tag{A 5a}$$

$$Pe\,\rho(u_z+U)\frac{\partial u_z}{\partial \xi} + \rho u_r\frac{\partial u_z}{\partial r} = -\frac{1}{Pe}\frac{\partial \bar{p}}{\partial \xi} + \frac{Pr}{Pe}\left[\frac{4Pe^2}{3}\left(\frac{\partial^2 u_z}{\partial \xi^2}\right) + \left(\frac{\partial^2 u_z}{\partial r^2}\right) + \frac{1}{r}\frac{\partial u_z}{\partial r} + \frac{Pe}{3r}\frac{\partial u_r}{\partial \xi} + \frac{Pe}{3}\left(\frac{\partial^2 u_r}{\partial \xi\,\partial r}\right)\right], \tag{A 5b}$$

$$Pe\,\rho(u_z+U)\frac{\partial u_r}{\partial \xi} + \rho u_r\frac{\partial u_r}{\partial r} = -\frac{1}{Pe^2}\frac{\partial \bar{p}}{\partial r} + \frac{Pr}{Pe}\left[\frac{4}{3}\left(\frac{\partial^2 u_r}{\partial r^2}\right) + Pe^2\left(\frac{\partial^2 u_r}{\partial \xi^2}\right) + \frac{4}{3r}\frac{\partial u_r}{\partial r} - \frac{4}{3}\frac{u_r}{r^2} + \frac{Pe}{3}\left(\frac{\partial^2 u_z}{\partial \xi\,\partial r}\right)\right], \tag{A 5c}$$

$$Pe^2\rho(u_z+U)\frac{\partial T}{\partial \xi} + Pe\,\rho u_r\frac{\partial T}{\partial r} = Pe^2\frac{\partial^2 T}{\partial \xi^2} + \frac{1}{r}\frac{\partial}{\partial r}\left(r\frac{\partial T}{\partial r}\right) + Pe^2 QR, \tag{A 5d}$$

$$Pe^2\rho(u_z+U)\frac{\partial Y}{\partial \xi} + Pe\,\rho u_r\frac{\partial Y}{\partial r} = \frac{1}{Le}\left(Pe^2\frac{\partial^2 Y}{\partial \xi^2} + \frac{1}{r}\frac{\partial}{\partial r}\left(r\frac{\partial Y}{\partial r}\right)\right) - Pe^2 R. \tag{A 5e}$$

In the limit $Pe \to 0$, solutions may be obtained with the expansions

$$T \sim T_0(\xi) + Pe^2 T_1(r,\xi), \quad Y \sim Y_0(\xi) + Pe^2 Y_1(r,\xi), \quad u_r \sim Pe\,u_{r0}(r,\xi), \tag{A 6}$$

$$u_z \sim u_{z0}(r,\xi) + O(Pe^2), \quad p \sim p_0(\xi) + O(Pe^2), \quad \rho \sim \rho_0(\xi) + O(Pe^2). \tag{A 7}$$

A separable solution for the leading-order axial velocity u_{z0} is again found. Its form is

$$u_{z0} = \tilde{u}_{z0}(\xi)(1-r^2), \tag{A 8}$$

corresponding to a Hagen–Poiseuille flow variation in the radial direction. The leading-order mass equation can be integrated from $r = 0$ to $r = 1$ where $u_{r0} = 0$ on $r = 0$ and $r = 1$ to give

$$\rho_0(\xi)\left(\frac{\tilde{u}_{z0}(\xi)}{2} + U_0\right) = \left(\frac{\tilde{u}_{z0u}}{2} + U_0\right) = M_p. \tag{A 9}$$

Following § 3, the leading-order radial velocity is determined to be

$$u_{r0} = \frac{r}{4\rho_0}\frac{\partial}{\partial \xi}\left(\rho_0\left(\tilde{u}_0(2-r^2) - 2U_0^2\right)\right), \tag{A 10}$$

while the leading-order vorticity magnitude is

$$|\omega| = -\frac{\partial u_{z0}}{\partial r} + O(Pe^2) = \tilde{u}_{z0}(\xi)2r + O(Pe^2). \tag{A 11}$$

As in § 3, the leading-order temperature and mass fraction variations can be obtained by integrating the $O(Pe^2)$ temperature and species equations from $r=0$ to $r=1$ to give

$$M_p \frac{\partial T_0}{\partial \xi} = \frac{\partial^2 T_0}{\partial \xi^2} - 2\kappa(T_0 - 1) + Q R_0(\xi) \tag{A 12}$$

and

$$M_p \frac{\partial Y_0}{\partial \xi} = \frac{1}{Le}\frac{\partial^2 Y_0}{\partial \xi^2} - R_0(\xi). \tag{A 13}$$

These equations are identical to those derived for channel flow, corresponding to variable-density one-dimensional flame propagation with volumetric heat loss, except that the heat loss factor in (A 12) is twice that found for channel flow.

For a flame opposed or assisted by a fully developed Hagen–Poiseuille flow as $\xi \to \infty$ (A 3c), $\tilde{u}_{z0u} = u_c$ and

$$U_0 = M_p - \frac{u_c}{2}. \tag{A 14}$$

Consequently, blow-off occurs for $u_c > 2M_p$. Whether or not blow-off is more easily achieved in a pipe ($u_c > 2M_p$) than in a channel ($u_c > 3M/2$) for the same flow conditions depends on the value of the heat loss coefficient κ. In an adiabatic channel, it is clearly harder to blow off a flame in a pipe ($u_c > 2$) than in a channel ($u_c > 3/2$). However, the doubling of the volumetric heat loss factor in (A 12) implies that M_p will be smaller than M for the channel case for fixed κ. When $M_p < 3M/4$, it is easier to blow off the flame in a pipe. The leading-order axial velocity variation is given by

$$\tilde{u}_{z0}(\xi) = u_c + 2M_p(T_0(\xi) - 1), \tag{A 15}$$

and $\tilde{u}_{z0}$ downstream of the flame ($\xi \to +\infty$) is given by

$$\tilde{u}_{z0b} = u_c + 2M_p(T_{0b} - 1), \tag{A 16}$$

where $T_{0b} = 1 + Q$ in the adiabatic case and $T_{0b} = 1$ in the non-adiabatic case. Thus $\tilde{u}_{z0b} = u_c + 2Q$ in the adiabatic case, a higher velocity than in the channel. For propagation away from the closed end of an adiabatic tube, where $\tilde{u}_{0zb} = 0$, the magnitude of centreline ($r=0$) induced flow as $\xi \to -\infty$ is consequently $u_c = -2Q$.

Finally, as in § 3, it is useful to calculate a measure of the $O(Pe^2)$ deformation induced on each surface of constant-mass fraction by the non-planar flow. The expression for Y is

$$Y \sim Y_0(\xi) + Pe^2\left(\frac{Le\,\rho_0 \tilde{u}_{z0}}{16}(2r^2 - r^4)\frac{\partial Y_0}{\partial \xi} + A(\xi)\right). \tag{A 17}$$

Let ξ^* be the location at which Y has the value Y^* in the leading-order problem. The $O(Pe^2)$ spatial perturbation at which Y now obtains the constant-mass fraction Y^* is given by

$$\xi' = \frac{Le\,\rho_0(\xi^*)\tilde{u}_{z0}(\xi^*)}{16}(r^4 - 2r^2) + B(\xi^*). \tag{A 18}$$

The relative distance between Y reaching the value Y^* on $r=0$ and $r=1$ is then given by

$$\xi'_{rp} = \frac{Le\,\rho_0 \tilde{u}_0}{16}, \tag{A 19}$$

where

$$\rho_0 \tilde{u}_{z0} = u_c + 2U_0(1-\rho_0) = \rho_0 u_c + 2M_p(1-\rho_0). \tag{A 20}$$

In an adiabatic channel, $M = M_p$ and

$$\xi'_r - \xi'_{rp} = \frac{\rho_0 \tilde{u}_c}{48}, \tag{A 21}$$

so that for $u_c \geqslant 0$ each surface of constant-mass fraction undergoes more deformation in the channel than the pipe. Finally, all of the generic characteristics of the influence of thermal expansion on flame propagation in a channel in the $Pe \to 0$ limit carry over to pipe flow.

REFERENCES

Chao, C. Y. H., Hui, K. S., Kong, W., Cheng. P. & Wang, J. H. 2007 Analytical and experimental study of premixed methane–air flame propagation narrow channels. *Intl J. Heat Mass Transfer* **50**, 1302–1313.

Clendening, J. C., Shackleford, W. & Hilyard, R. 1981 Raman scattering measurement in a sidewall quench layer. *Proc. Combust. Inst.* **18** 1583–1589.

Cui, C., Matalon, M., Daou, J. & Dold, J. 2004 Effects of differential diffusion on thin and thick flames propagating in channels. *Combust. Theory Model.* **8**, 41–64.

Cui, C., Matalon, M. & Jackson, T. L. 2005 Pulsating mode of flame propagation in two-dimensional channels. *AIAA J.* **43**, 1284–1292.

Daou, J. & Matalon, M. 2001 Flame propagation in Poiseuille flow under adiabatic conditions. *Combust. Flame* **124**, 337–349.

Daou, J. & Matalon, M. 2002 Influence of conductive heat-losses on the propagation of premixed flames in channels. *Combust. Flame* **128**, 321–329.

Dobrego, K. V., Kozlov, I. M. & Vasiliev, V. V. 2006 Flame dynamics in thin semi-closed tubes at different heat loss conditions. *Intl J. Heat Mass Transfer* **49**, 198–206.

Fernandez-Pello, A. C. 2002 Micropower generation using combustion: issues and approaches. *Proc. Combust. Inst.* **29**, 883–899.

Gamezo, V. N. & Oran, E. S. 2006 Flame acceleration in narrow channels: applications for micropropulsion in low-gravity environments. *AIAA J.* **44**, 329–336.

Hackert, C. L., Ellzey, J. L. & Ezekoye, O. A. 1998 Effects of thermal boundary conditions on flame shape and quenching in ducts. *Combust. Flame* **112**, 73–84.

Jackson, T. L., Buckmaster, J., Lu, Z., Kyritsis, D. C. & Massa, L. 2007 Flames in narrow circular tubes. *Proc. Combust. Inst.* **31**, 955–962.

Jones *et al.* 1978 Combustion in heat-exchangers. *Proc. R. Soc. Lond.* A **360**, 97–115.

Ju, Y. G. & Xu, B. 2005 Theoretical and experimental studies on mesoscale flame propagation and extinction. *Proc. Combust. Inst.* **30**, 2445–2453.

Kessler, D. A. 2006 Edge-flames and combustion at the microscale. PhD thesis, University of Illinois at Urbana-Champaign, Urbana, IL.

Kurdyumov, V. N. & Fernandez-Tarrazo, E. 2002 Lewis number effect on the propagation of premixed laminar flames in narrow open ducts. *Combust. Flame* **128**, 382–394.

Leach, T. T. & Cadou, C. P. 2005 The role of structural heat exchange and heat loss in the design of efficient silicon micro-combustors. *Proc. Combust. Inst.* **30**, 2437–2444.

Lewis, B. & von Elbe, G. 1961 *Combustion, Flames and Explosions of Gases.* Academic.

Liu, Y. 2003 Flames in thin channels. PhD thesis, University of Illinois at Urbana-Champaign, Urbana, IL.

Kessler, D. A. & Short, M. 2008 Ignition and transient dynamics of sub-limit premixed flames in microchannels. *Combust. Theory Model.* **12**, 809–829.

Kim, N. I. & Maruta, K. 2006 A numerical study on propagation of premixed flames in small tubes. *Combust. Flame* **146**, 283–301.

Maruta, K., Kataoka, T., Kim, N. I., Minaev, S. & Fursenko, R. 2005 Characteristics of combustion in a narrow channel with a temperature gradient. *Proc. Combust. Inst.* **30**, 2429–2436.

Miesse, C. M., Masel, R. I., Jensen, C. D., Shannon, M. A. & Short, M. 2004 Submillimeter-scale combustion. *AIChE J.* **50**, 3206–3214.

Mineav, S., Maruta K. & Fursenko, R. 2007 Nonlinear dynamics of flame in a narrow channel with a temperature gradient. *Combust. Theory Model.* **11**, 187–203.

Norton, D. G. & Vlachos, D. G. 2003 Combustion characteristics and flame stability at the microscale: a CFD study of premixed methane/air mixtures. *Chem. Engng Sci.* **58**, 4871–4882.

Ott, J. D., Oran, E. S. & Anderson, J. D. 2003 A mechanism for flame acceleration in narrow tubes. *AIAA J.* **41**, 1391–1396.

Ronney, P. D. 2003 Analysis of non-adiabatic heat-recirculating combustors. *Combust. Flame* **135**, 421–439.

Short, M. & Kessler, D. A. 2009. Variable density premixed flame propagation in a microchannel with heat conducting axial walls. Combust. Theory Modell., Submitted.

Tsai, C. H. 2008 The asymmetric behaviour of steady laminar flame propagation in ducts. *Combust. Sci. Technol.* **180**, 533–545.

Williams, F. A. 1985 *Combustion Theory*. Westview Press.

Zamashchikov, V. V. 2001 An investigation of combustion in a narrow tube. *Combust. Sci. Technol.* **166**, 1–14.

Zamashchikov, V. V. & Minaev, S. S. 2001 Limits of flame propagation in a narrow channel with gas filtration. *Combust. Exp. Shock Waves* **37**, 21–26.